

# A quantum theory for nuclear spin dynamics induced electron spin decoherence in semiconductor quantum computer architectures: Spectral diffusion of localized electron spins in the nuclear solid state environment

W.M. Witzel<sup>1</sup> and S. Das Sarma<sup>1</sup>

<sup>1</sup>*Condensed Matter Theory Center, Department of Physics,  
University of Maryland, College Park, MD 20742-4111*

(Dated: May 24, 2019)

We consider the decoherence of a single localized electron spin due to its coupling to the lattice nuclear spin bath in a semiconductor quantum computer architecture. In the presence of an external magnetic field and at low temperatures, the dominant decoherence mechanism is the spectral diffusion of the electron spin resonance frequency due to the temporally fluctuating random magnetic field associated with the dipolar interaction induced flip-flops of nuclear spin pairs. The electron spin dephasing due to this random magnetic field depends intricately on the quantum dynamics of the nuclear spin bath, making the coupled decoherence problem difficult to solve. We provide an exact solution of this non-Markovian quantum decoherence problem. A quantum cluster expansion method is introduced for the problem of localized electron spin decoherence due to dipolar fluctuations of lattice nuclear spins. At the lowest order it provides a microscopic explanation for the Lorentzian diffusion of Hahn spin echoes without resorting to any phenomenological Markovian assumption. The quantum cluster expansion method is developed, justified, and tested for the problem of localized electron spin decoherence due to dipolar fluctuations of lattice nuclear spins. The method is presented with enough generality for possible application to other types of spin decoherence problems. We also describe techniques to obtain an algebraic time expansion of the spin echo decoherence computationally. This time expansion has limited applicability but is used for independent verification of our cluster expansion. We present numerical results which are in quantitative agreement with electron spin echo measurements in phosphorus doped silicon. We also present spin echo decay results for quantum dots in GaAs which differ qualitatively from that of the phosphorus doped silicon system. Our theoretical results provide the ultimate limit on the spin coherence (at least, as characterized by Hahn spin echo measurements) of localized electrons in semiconductors in the low temperature and the moderate to high magnetic field regime of interest in scalable semiconductor quantum computer architectures.

PACS numbers: 76.30.-v; 03.65.Yz; 03.67.Pp; 76.60.Lz

## I. INTRODUCTION

Quantum computation considerations have generated a great deal of recent interest in the old<sup>1,2,3,4,5,6</sup> problem of electron spin coherence in semiconductors. In particular, a localized electron spin can act as a qubit (i.e. a quantum dynamical 2-level system) for quantum information processing in scalable solid state quantum computer architectures.<sup>7,8</sup> But using such spin qubits for quantum information processing purposes necessarily requires long spin coherence time, and therefore understanding electron spin decoherence in the solid state environment becomes a key issue. In this article, we develop a quantum theory for, what we consider to be, the most important electron spin decoherence mechanism in spin-qubit based semiconductor quantum computer architectures. The spin decoherence mechanism we consider here is the so-called spectral diffusion mechanism, which has a long history,<sup>1,2,3,4,5,6</sup> and has been much-studied recently<sup>9,10,11,12,13</sup> in the context of spin qubit decoherence.

To provide a physical background for the theory to be presented in this paper we start by considering a localized electron in a solid, for example a donor-bound

electron in a semiconductor as in the doped Si:P system. Such a Si:P system is the basis of the Kane quantum computer architecture.<sup>7</sup> The electron spin could decohere through a number of mechanisms. In particular, spin relaxation would occur via phonon or impurity scattering in the presence of spin-orbit coupling, but these relaxation processes are strongly suppressed in localized systems and can be arbitrarily reduced by lowering the temperature. In the dilute doping regime of interest in quantum computation, where the localized electron spins are well-separated spatially, direct magnetic dipolar interaction between the electrons themselves is not an important dephasing mechanism.<sup>14</sup> Interaction between the electron spin and the nuclear spin bath is therefore the important decoherence mechanism at low temperatures and for localized electron spins. Now we restrict ourselves to a situation in the presence of an external magnetic field (which is the situation of interest to us in this paper) and consider the spin decoherence channels for the localized electron spin interacting with the lattice nuclear spin bath. Since the gyromagnetic ratios (and hence the Zeeman energies) for the electron spin and the nuclear spins are typically a factor of 2000 different (the electron Zeeman energy being larger), hyperfine coupling induced direct spin-flip transitions between electron and nuclear spins

would be impossible at low temperature since phonons would be required for energy conservation. Thus, finite magnetic fields and low temperatures would in general strongly suppress hyperfine coupling induced electron spin relaxation, which is an effective process at zero magnetic field. This leaves the indirect spectral diffusion mechanism as the most effective electron spin decoherence mechanism at low temperatures and finite magnetic fields. The spectral diffusion process is associated with the dephasing of the electron spin resonance due to the temporally fluctuating nuclear magnetic field at the localized electron site. These temporal fluctuations cause the electron spin resonance frequency to diffuse in the frequency space, hence the name spectral diffusion. We note that the (hyperfine) coupling between the electron spin and the nuclear spin bath implies that any mechanism leading to the decoherence of nuclear spins (either a  $T_1$ -type spin relaxation or a  $T_2$ -type spin dephasing) would, in principle, produce spectral diffusion in the electron spin, i.e. give rise to a  $T_2$ -type spin dephasing mechanism in the electron spin. The specific electron spin spectral diffusion process being considered in this work is that arising from the magnetic dipolar interaction induced flip-flop mechanism in nuclear spins leading to random temporal fluctuations in the electron spin resonance frequency. Other local flip-flop mechanisms between nuclei, such as indirect exchange interactions<sup>15,16,17</sup> (which we will briefly address in this article in the context of GaAs), may be easily included in our formalism. We do not, however, treat the non-local hyperfine-mediated interactions (resulting from virtual spin-flip transition between hyperfine-coupled electron and nuclear spins), which, under the application of refocusing pulses, lead only to a small visibility decay and can be reduced by increasing the strength of the external magnetic field.<sup>18</sup> We thus treat the only spectral diffusion phenomena of any quantitative significance in the semiconductor-based solid state spin quantum computer architectures of interest to us, namely, the dipolar interaction induced nuclear spin flip-flop dynamics in the solid state environment.

The spectral diffusion is a theoretically challenging problem because the temporally fluctuating random field causing the electron spin dephasing is a non-Markovian stochastic dynamical variable arising from the complex dipolar quantum dynamics of a large number of interacting nuclear spins. Although the spectral diffusion is an intrinsic dephasing mechanism contributing to the so-called  $T_2$ -type (i.e. “transverse”) spin decoherence in the phenomenological Bloch equation language, the effect of spectral diffusion on the electron spin dynamics (for example, on the electron spin resonance measurement) cannot be characterized by a simple relaxation (or dephasing) time  $T_2$  associated with a ‘trivial’  $e^{-t/T_2}$  type of temporal loss of coherence. The non-Markovian nuclear spin bath dynamics produces a rather complex electron spin dephasing which cannot be characterized by a single decoherence time (except as a very crude approximation). It is therefore more appropriate to consider spectral dif-

fusion in the context of a specific experimental situation, and it has been traditional, going back to the seminal pioneering work of Hahn, to study spectral diffusion in the context of the spin echo decay in pulsed spin resonance measurements.<sup>1,19</sup> In spin echo measurements, the inhomogeneous broadening effects are suppressed by design, and any amplitude decay in the consecutive pulses arises entirely from the  $T_2$ -dephasing time associated with spectral diffusion (and, of course, other applicable  $T_2$ -type transverse relaxation processes).

It was realized a long time ago<sup>1,4</sup> that spectral diffusion due to the dipolar fluctuations of nuclear spins often dominates the coherence decay in electron spin echo experiments. All available theories to date are based on classical stochastic modeling of the nuclear field, a Markovian theoretical framework which is inevitably phenomenological since it requires an arbitrary choice for the spectrum of nuclear fluctuations. Such a classical Markovian modeling is arguably incompatible with the strict requirements of spin coherence and control in a quantum information device. In addition, recent rapid experimental progress in single spin measurements,<sup>20</sup> which in the near future promises sensitive measurements of quantum effects in spin resonance, also warrants a quantum theory of spectral diffusion. In the current work, we develop a quantum theory of spin echo decay in electron spin resonance experiments due to the spectral diffusion caused by the dipolar interaction induced flip-flop nuclear spin dynamics. We emphasize that, in contrast to all the earlier theories of spectral diffusion in the literature, our theory is fully quantum mechanical and incorporates the dipolar nuclear spin flip-flop dynamics microscopically without making any phenomenological statistical (Markovian or otherwise) approximations. In addition, our theory produces an accurate quantitative prediction of the Hahn echo decay. To the best of our knowledge, ours is the first fully quantum theory for electron spin spectral diffusion in solid state systems.

Spectral diffusion is, in principle, not a limiting decoherence process for silicon or germanium based quantum computer architectures because these can, in principle, be fabricated free of nuclear spins using isotopic purification. Unfortunately this is not true for the important class of materials based on III-V compounds, where spectral diffusion has been shown to play a major role.<sup>9,14</sup> There is as yet no direct (e.g. GaAs quantum dots) experimental measurement of localized spin dephasing in III-V materials, but such experimental results are anticipated in the near future. Indirect spin echo measurements based on singlet-triplet transitions in coupled GaAs quantum dot systems<sup>21</sup> give  $T_2$  times consistent with our theoretical results.

Our theory reveals that the inclusion of quantum corrections to nuclear spin fluctuation increases the degree of decoherence at lower to intermediate time scales, as is best evidenced from our explanation of the existing factor of three discrepancy between the Markovian stochastic theory<sup>9</sup> and experimental data<sup>6,10,11</sup> of spin echo de-

decay in phosphorus doped silicon. Our method allows a fully microscopic explanation for the observed time dependence of Hahn echo decay due to a nuclear spin environment. It was pointed out a long time ago<sup>4,6,11</sup> that the observed time dependence of these echoes are well fitted to the expression  $\exp(-\tau^2)$  (here  $\tau$  is half of the time lag between the initial signal and an echo), a behavior which can be derived phenomenologically<sup>4</sup> by assuming Lorentzian Brownian motion for the electron spin Zeeman frequency. In our method this behavior arises naturally from the collective quantum evolution of the dipolar coupled nuclei, without any phenomenological assumption on the dynamics of the environment responsible for decoherence. A proper description of coupled spin dynamics is rather difficult due to the absence of the usual Wick's theorem for spin degrees of freedom. In that regard, variations of our method may prove rather useful, since environmental spin baths are ubiquitous in any device exploiting the coherent properties of quantum spin systems.

The rest of this article is organized as follows. In section II we provide a brief background for the spectral diffusion process; in section III we formulate the theoretical problem of spectral diffusion in the context of Hahn spin echo decay; in section IV we develop and describe the quantum cluster expansion which is the important new theoretical result of our work; in section V we describe the dual perturbation theories in terms of a  $\tau$ -expansion and a dipolar perturbation expansion justifying the convergence of our cluster expansion and providing independent verification of its validity; and finally in section VI we apply our theory to obtain numerical results. We conclude in section VII. Three appendices provide some mathematical details.

## II. BACKGROUND

Spectral Diffusion (SD) is a spin decoherence mechanism caused by fluctuations in a spin's Zeeman frequency, leading to dephasing. In general, these fluctuations can be a result of any cause such as random fluctuations in the external magnetic field. Our interest, however, is in processes at low temperatures and in a high magnetic field, relevant for solid state quantum computing architectures. In these systems, a localized electron spin serving as the qubit has a wave function that typically envelopes hundreds of thousands of nuclei or more in the surrounding neighborhood of the lattice. Two such examples are the shallow donor electron state in a phosphorus dopant in silicon<sup>7</sup> and a localized electron in a quantum dot in GaAs<sup>8</sup>. A schematic<sup>22</sup> of the spectral diffusion process in the former is shown in Fig. 1. In these systems, where donors or dots are sparse such that interactions between them can be ignored, the dominant decoherence method, with spin-lattice relaxation processes frozen out in the low temperature, is the SD caused by the dynamic evolution of nuclear spins resulting in effective magnetic

## Spectral diffusion of a Si:P spin

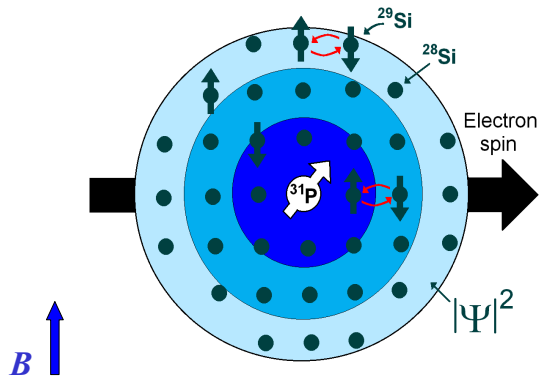


FIG. 1: The electron of a phosphorus donor in silicon experiences spectral diffusion due to a bath of nuclear spins in the enveloped silicon. The majority of natural silicon is  $^{28}\text{Si}$  which has no valence spin and does not contribute to SD. The remainder (about 5% for natural silicon, or less if isotopically purified) are  $^{29}\text{Si}$  which have an effective nuclear spin of  $1/2$  and do contribute. The dominant contribution is from the flip-flop process of neighboring  $^{29}\text{Si}$  pairs. Spectral diffusion can be suppressed in Si:P by isotopical purification or nuclear spin polarization.

field fluctuations experienced by the electron. The electron spin couples to nuclear spins via hyperfine interaction in the region in which the electron wave function is appreciable. The nuclear spins couple to each other via dipolar interactions. The large external field suppresses processes that do not conserve electron or nuclear spin polarization in the direction of the magnetic field. Thus the only relevant nuclear processes are flip-flops in which one spin is raised while the other is lowered.

SD is a dephasing decoherence (i.e. a transverse or  $T_2$ -type relaxation) process, affecting only the precession of the electron spin in the Bloch sphere without changing the electron spin component along the magnetic field. It thus contributes to the energy-conserving  $T_2$  decoherence rather than  $T_1$  decoherence in which energy is exchanged with the bath (Ref. [23] details our definition of  $T_1$ ,  $T_2$ , and  $T_2^*$ ). The  $T_1$  time for these systems at low temperature is known to be much longer than this  $T_2$  time. To analyze this decoherence, we consider an ensemble of spins, initialized in some direction perpendicular to the magnetic field, and observe the decay of the average spin over time. In experiments, many sparse donors or dots serve as the ensemble, and they are initialized by applying a  $\pi/2$ -pulse to rotate electron spins polarized along the magnetic field axis into the plane perpendicular to the magnetic field. For the free induction decay (FID), no further pulses are applied and the observed decay is largely due to inhomogeneous broadening which is caused by the difference in the local magnetic field of each elec-

tron, causing precession at different rates for different electrons. This will provide what is referred to as the  $T_2^*$  decoherence time. At the very least, this inhomogeneous broadening is a result of the random initial distribution of nuclear spin states which gives an uncertainty that scales as  $\sqrt{N}$  where  $N$  is the effective number of nuclei ( $\sim 10^6$  typically in the semiconductor quantum computer architecture) influencing the electron significantly. This decoherence due to inhomogeneous broadening can be eliminated by refocusing methods such as the Hahn echo.<sup>19</sup> In such an experiment, a  $\pi$ -pulse, resonant with electron spins, is applied at time  $t = \tau$  in the same direction as the original  $\pi/2$  pulse and then an echo is observed at  $t = 2\tau$ . This has the effect of reversing any static local field effects and allows us to obtain the actual SD decoherence (i.e. the  $T_2$  decoherence as opposed to  $T_2^*$  decoherence) caused by effective magnetic field fluctuations. This experiment provides a measure of  $T_2$ . The current paper will analyze the Hahn echo experiment. More sophisticated pulses, such as the Carr-Purcell-Meiboom-Gill sequence,<sup>24</sup> can yield even longer decoherence times and will be analyzed in future publications.

Previous attempts at analyzing this SD decoherence have been based on quasi-classical stochastic modeling. Herzog and Hahn<sup>1</sup> assigned a phenomenological Gaussian probability distribution function for the Zeeman frequency of the investigated spin without considering the dynamics of the nuclear bath. Later, Klauder and Anderson<sup>4</sup> used a Lorentzian distribution function instead in order to account for a power law time dependence observed in experiments by Mims and Nassau<sup>3</sup>. Zhidomirov and Salikhov<sup>5</sup> devised a more sophisticated theory, with a wider range of applicability, in which the number of flips during a time interval of each spin in the bath was characterized by Poisson distributions. Very recently de Sousa and Das Sarma<sup>9</sup>, in considering spectral diffusion by nuclear spin flip-flops, extended this theory to characterize flip-flop rates of pairs rather than individual spins within a phenomenological model.

In this paper, we present a microscopic theory that is based entirely on the quantum mechanics of the system without resorting to phenomenological distribution functions. No Markovian assumption nor any assumption about the form of the solution was used to obtain our results here. Our expansion is entirely based upon a density matrix formulation of the problem which assumes infinite nuclear spin temperature ( $T \gg \text{nK}$ ) and uses an approximate but microscopic Hamiltonian. The problem obviously involves too many nuclear spins to solve directly using exact Hamiltonian diagonalization; however, the cluster expansion method we devise can give successive approximations to the exact solution. A short report of our results without any theoretical details has earlier appeared as a Rapid Communication [12]. Our lowest order solution<sup>12</sup> was recently reproduced by Yao *et al*<sup>13</sup> using an entirely different approach, thus providing an independent validation of our theoretical approach.

### III. FORMULATION OF THE PROBLEM

#### A. Free evolution Hamiltonian

The free evolution Hamiltonian for the spectral diffusion problem, considering one localized electron spin,  $S$ , and a nuclear spin bath,  $\mathbf{I}_n$ , in an external magnetic field  $B$  (taken to be along the  $z$ -direction), is given by

$$\mathcal{H} = \mathcal{H}_{Ze} + \mathcal{H}_{Zn} + \mathcal{H}_A + \mathcal{H}_B, \quad (1)$$

where the first two terms are due to the Zeeman energies of the electron and nuclei respectively,  $\mathcal{H}_A$  gives the electron-nuclei coupling, and  $\mathcal{H}_B$  contains the inter-nuclear coupling.

The Zeeman energy contributions, arising from the external magnetic field, are given by,

$$\mathcal{H}_{Ze} = \gamma_S BS_z, \quad (2)$$

$$\mathcal{H}_{Zn} = -B \sum_n \gamma_n I_{nz}, \quad (3)$$

where  $\gamma_S$  and  $\gamma_n$  are the gyromagnetic ratios of the electron spin and nuclear spins respectively, and  $B$  is the external magnetic field defined to point in the  $z$  direction.

The electron-nuclei coupling is given by,

$$\mathcal{H}_A = \sum_n A_n (I_n \cdot S). \quad (4)$$

$A_n$  gives the magnetic coupling between the electron spin and each nuclear spin. It is dominated by the hyperfine coupling for nuclei that contribute significantly to SD. Since  $\gamma_S = 1.76 \times 10^7 (\text{s G})^{-1}$  is typically four orders of magnitude larger than  $\gamma_n$ , flip-flop processes between the electron and a nuclear spin are strongly suppressed at low temperatures (i.e. no phonons) by energy conservation in a strong magnetic field. This direct hyperfine interaction leads to quantitatively important effects at zero magnetic field,<sup>25</sup> but at the moderate or high magnetic fields required for spin resonance measurements it only contributes a small visibility decay<sup>26</sup>. An exception is the non-local hyperfine-mediated coupling between nuclei in which these electron-nuclei flip-flops occur as a higher order virtual process. However, apart from a small visibility decay, the effect from this process is canceled out in the Hahn echo that we analyze in this paper.<sup>13,18</sup> We will therefore disregard the non-secular part of the electron-nuclei coupling, leaving us with,

$$\mathcal{H}_A \approx \sum_n A_n I_{nz} S_z, \quad (5)$$

which we will use as the definition for  $\mathcal{H}_A$  throughout the rest of this paper.

The inter-nuclear coupling due to the dipolar interaction is given by,<sup>27</sup>

$$\mathcal{H}_B = \frac{1}{2} \sum_{n \neq m} \gamma_n \gamma_m \hbar \left[ \frac{\mathbf{I}_n \cdot \mathbf{I}_m}{R_{nm}^3} - \frac{3(\mathbf{I}_n \cdot \mathbf{R}_{nm})(\mathbf{I}_m \cdot \mathbf{R}_{nm})}{R_{nm}^5} \right], \quad (6)$$

where  $\mathbf{R}_{nm}$  is the vector joining nuclei  $n$  and  $m$ . This can be expanded into a form containing only operators of the type  $I_+$ ,  $I_-$ , or  $I_z$ .<sup>27</sup> We will again invoke the energy conservation argument which, because of the strong external magnetic field, allows us to neglect any term that changes the total Zeeman energy of the nuclei. This will leave us with the following secular contribution,

$$\mathcal{H}_B \approx \sum_{n \neq m} b_{nm}(\delta(\gamma_n - \gamma_m)I_{n+}I_{m-} - 2I_{nz}I_{mz}), \quad (7)$$

$$b_{nm} = -\frac{1}{4}\gamma_n\gamma_m\hbar\frac{1 - 3\cos^2\theta_{nm}}{R_{nm}^3}. \quad (8)$$

Eq. (7) will be used for  $\mathcal{H}_B$  throughout the rest of this paper. Note that the flip-flop interaction between nuclei with different gyromagnetic ratios is suppressed by Zeeman energy conservation in the same way that the non-secular part of the dipolar interaction is suppressed. This occurs, for example, in GaAs because the two isotopes of Ga and the one isotope of As that are present have significantly different gyromagnetic ratios. This approximation is applicable if any such differences in  $\gamma_n$  are on the order of  $|\gamma_n|$  itself and thus such energy changes would be large compared to other energies of the problem in the large external magnetic field being considered in this work. Giving some typical numbers,  $\text{Max}(|A_n|) \sim 10^6 s^{-1}$ ,  $\text{Max}(|b_{nm}|) \sim 10^2 s^{-1}$ , and for  $B = 10$  T,  $|\gamma_n B| \sim 10^8 s^{-1}$  and  $|\gamma_S B| \sim 10^{12} s^{-1}$ . The Zeeman energies are thus much larger than the other energies in the problem. In fact, our model of neglecting terms that change the total Zeeman energy of the nuclei turns out to be reasonably valid for  $B > 0.1$  T or so for Si:P or GaAs systems of interest to us. The SD is therefore the dominant spin decoherence channel for localized electrons in semiconductors except at zero or very small ( $< 0.1$  T) magnetic fields.

## B. Hahn echo

The Hahn echo experiment consists of preparing the electron spin in a state perpendicular to the magnetic field, allowing free evolution for a time  $\tau$ , applying an electron spin resonant  $\pi$ -pulse about an axis perpendicular to the magnetic field (for our theoretical purpose, the direction of this axis is not important beyond being perpendicular to the  $B$ -field), and then allowing free evolution again for time  $\tau$ . The echo envelope is the magnitude of the resulting ensemble spin average at time  $t = 2\tau$ .

Mathematically, the echo envelope  $v_E(\tau)$ , echo as a function of  $\tau$ , may be written

$$v_E(\tau) = 2\sqrt{|\langle S_x \rangle|^2 + |\langle S_y \rangle|^2} \quad (9)$$

$$= 2|\text{Tr}\{(S_x + iS_y)\rho(\tau)\}|, \quad (10)$$

The factor of 2 normalizes the echo to one at  $\tau = 0$  since the electron has a spin of 1/2. The density matrix of the

system,  $\rho(\tau)$ , is given by

$$\rho(\tau) = U(\tau)\rho_0U^\dagger(\tau), \quad (11)$$

with the evolution operator

$$U(\tau) = e^{-i\mathcal{H}\tau}\sigma_{x,e}e^{-i\mathcal{H}\tau}, \quad (12)$$

where  $\mathcal{H}$  is the free evolution Hamiltonian given by Eq. (1). We have arbitrarily chosen the pulse axis to be in the  $x$  direction. This pulse is represented by the Pauli matrix,  $\sigma_{x,e} = 2S_x$  with the  $e$  subscript denoting that it is an electron spin operator.

Our initial density matrix,  $\rho_0$ , will be given by a product state of the electron spin in a direction perpendicular to the magnetic field and the nuclear spins in a thermal state,

$$\rho_0 = |\chi_e^0\rangle\langle\chi_e^0| \otimes \frac{e^{-\mathcal{H}_n/k_B T}}{M}, \quad (13)$$

$$|\chi_e^0\rangle = \frac{1}{\sqrt{2}}(|0_e\rangle + e^{i\phi}|1_e\rangle), \quad (14)$$

where  $\mathcal{H}_n = \mathcal{H}_{Zn} + \mathcal{H}_B$  and  $M$  is its partition function ( $M \approx 2^N$  for  $T \gg nK$ ,<sup>9</sup> where  $N$  is the number of nuclear spins). In our formulation, with the absolute value taken in Eq. (10),  $\phi$  will be irrelevant. After a few manipulations, shown in Appendix A, Eq. (10) becomes

$$v_E(\tau) = \frac{1}{M} \left| \text{Tr} \left\{ U_- U_+ e^{-\mathcal{H}_n/k_B T} U_-^\dagger U_+^\dagger \right\} \right|, \quad (15)$$

where

$$U_\pm = e^{-i\mathcal{H}_\pm\tau}, \quad (16)$$

are evolution operators under the effective Hamiltonians

$$\mathcal{H}_\pm = \mathcal{H}_B \pm \frac{1}{2} \sum_n A_n I_{nz}, \quad (17)$$

which describe nuclear evolution under the effect of an electron spin up ( $\mathcal{H}_+$ ) or down ( $\mathcal{H}_-$ ) with the external magnetic field dependence now canceled out. Although the  $U_\pm$  evolution operators are independent of  $B$ , it should be noted that a strong external magnetic field is required to justify the approximations of Eqs. (5) and (7). The trace in Eq. (15) is taken over nuclear spin states only.

For our purposes we only consider high nuclear temperatures ( $T \gg nK$ ) such that we can make the following approximation,

$$v_E(\tau) = \frac{1}{M} \left| \text{Tr} \left\{ U_- U_+ U_-^\dagger U_+^\dagger \right\} \right|. \quad (18)$$

The high nuclear temperature (and the low electron and phonon temperature) approximation made throughout this work is well-valid in the solid state quantum computer architectures of our interest, where typical experiments would be carried out around  $T \sim 100$  mK which is an extremely high temperature for the nuclear bath dynamics and an extremely low temperature for phonon excitations.

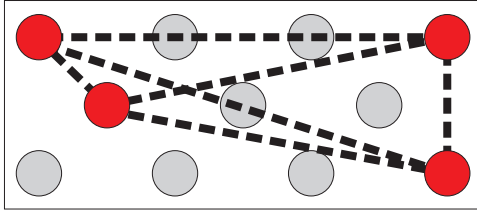


FIG. 2: This schematic representation of an arbitrary subset conveys the fact that constituent nuclei of a subset need not be in close proximity to each other (unlike clusters which are soon to be discussed). The circles represent nuclei. The red/dark circles denote nuclei contained in this subset with dashed lines representing possible interactions between them (which may be negligible between distant pairs).

#### IV. CLUSTER METHOD

Before giving any specific justification for our methodology, we will discuss our cluster approach in somewhat general terms and discuss the conditions in which it is appropriate to use. There are three conditions needed to formulate a cluster expansion using our method. First, we must have a large system, of size  $N$ , in which a near neighbor approximation is applicable. In our case  $b_{nm} \sim 1/R^3$  [Eq. (8)] justifies a near neighbor approximation. Second, we must be able to compose our desired solution from a sum of “subset contributions” for all possible subsets of the  $N$  items (nuclei in our case). Finally, we must show that larger subsets will provide smaller contributions than smaller subsets by orders of some  $\lambda \ll 1$ . Such a  $\lambda$  is related to a perturbation expansion to be explained and described later in this paper. Our cluster approach, which is shown below for this problem specifically, is motivated by the fact that a direct application of such a perturbation expansion may not be valid when  $\lambda N \gg 1$ , but a cluster approach would still be valid.

Let us decompose  $v_E(\tau)$  into terms that involve different subsets of the nuclei. Let  $\mathcal{D}$  be a subset of the nuclei in the problem (shown schematically in Fig. 2). Let  $v'_{\mathcal{D}}(\tau)$  be the sum of terms in some fully distributed expansion of  $v_E(\tau)$  that involve *only* and *all* of the nuclei in subset  $\mathcal{D}$ . We call  $v'_{\mathcal{D}}(\tau)$  the “subset contribution” from subset  $\mathcal{D}$ . In accordance with the second criterion stated above, our desired solution is composed of “subset contributions” from all possible subsets:

$$v_E(\tau) = \sum_{\mathcal{D}} v'_{\mathcal{D}}(\tau). \quad (19)$$

Obviously, Eq. (19) is formally an identity and its utility will emerge, as we shall soon show, from ordering the importance of  $v'_{\mathcal{D}}(\tau)$  for different subsets,  $\mathcal{D}$ .

Now let  $v_{\mathcal{D}}(\tau)$  be the solution to  $v_E(\tau)$  when only including the nuclei in subset  $\mathcal{D}$ . Without needing to delve into unimportant details, we know that  $v_{\mathcal{D}}(\tau)$  is a function that “involves” nuclei only via  $\mathcal{H}_{\pm}$ . Therefore, the

only role of  $\mathcal{D}$  in  $v_{\mathcal{D}}(\tau)$  is to define the range of the sums in Eqs. (17) and (7). The “contribution” of subset  $\mathcal{S} \subseteq \mathcal{D}$  to  $v_{\mathcal{D}}(\tau)$  is thus independent of  $\mathcal{D}$  (one would only distribute through terms in these sums that involve elements of  $\mathcal{S}$ ). We may therefore write  $v_{\mathcal{D}}(\tau)$  as the sum of its subset contributions:

$$v_{\mathcal{D}}(\tau) = \sum_{\mathcal{S} \subseteq \mathcal{D}} v'_{\mathcal{S}}(\tau), \quad (20)$$

with the knowledge that  $v'_{\mathcal{S}}(\tau)$  is independent of  $\mathcal{D}$ . From this it is easy to obtain a recursive expression for any “subset contribution”:

$$v_{\mathcal{D}}(\tau) = v'_{\mathcal{D}}(\tau) + \sum_{\mathcal{S} \subset \mathcal{D}} v'_{\mathcal{S}}(\tau), \quad (21)$$

$$v'_{\mathcal{D}}(\tau) = v_{\mathcal{D}}(\tau) - \sum_{\mathcal{S} \subset \mathcal{D}} v'_{\mathcal{S}}(\tau). \quad (22)$$

For the empty set,  $v'_{\emptyset}(\tau) = v_{\emptyset}(\tau) = 1$ .

For now, we will simply assume that a subset of size  $k$  will give a contribution of  $O(\lambda^k)$  where  $\lambda \ll 1$  (the third criterion for our cluster expansion). We will later justify this by relating  $\lambda$  to two perturbation expansions that are valid in complementary regimes for the spectral diffusion problem. We again write  $v_E(\tau)$  as a sum of contributions from all possible subsets, this time ordered by subset size:

$$v_E(\tau) = 1 + \sum_{k=2}^{k_0} \sum_{|\mathcal{D}|=k} v'_{\mathcal{D}}(\tau) + O(\lambda^{k_0+1}), \quad (23)$$

where the second summation is over all possible nuclear subsets of size  $k$  (containing  $k$  distinct nuclear sites). We note that a subset of size one gives no contribution because an isolated nucleus in our model does not contribute to spectral diffusion. This conclusion may also be drawn by an examination of Eq. (22) with  $|\mathcal{D}| = 1$  and Eq. (18) when only a single nucleus is included.

The  $O(\lambda^{k_0+1})$  error in Eq. (23) is misleading because the number of terms of a given order of  $\lambda$  may be large compared to  $\lambda$ . The nature of this problem, as well as a solution, becomes apparent when we invoke a near neighbor approximation. With this approximation, we ignore the interaction between distant nuclei (i.e. pairs of nuclei for which  $b_{nm}$  is below some threshold) and let the average number of “neighbors” for each nucleus be  $L \ll N$ . We can then divide our nuclear subsets into connected “clusters.” As proven in Appendix B, a subset contribution is simply the product of its cluster contributions. We note that while the “subset” is a purely formal decomposition, the “cluster” decomposition is physically motivated by the actual details of our spectral diffusion problem and depends critically on the near neighbor structure of the system.

The problem with Eq. (23) is that the number of terms grows roughly in orders of  $N \gg 1$  as we increase subset size. If we revise the expansion of Eq. (23) in terms of

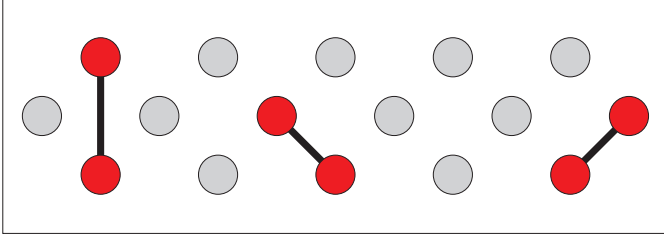


FIG. 3: This is a schematic of a subset composed entirely of pair clusters. The circles denote nuclei. The red/dark circles are the nuclei contained in this subset. The only non-negligible interactions between members of this subset, represented as solid lines, are between the pairs.

cluster sizes rather than subset sizes, we can keep these orders of  $N$  in check with orders of  $\lambda$  because the number of clusters of size  $k$  is  $O(NL^{k-1})$ , always linear in  $N$ . At the lowest order of this new expansion will be the contributions of all subsets composed entirely of pair clusters (clusters of one give no contribution). A schematic of such a subset is shown in Fig. 3. At the next order we will have subsets composed of pairs and/or triplets. The next order introduces clusters of four, etc. Of course, it would be an extremely arduous task to sum over all possible combinations of pairs, triplets, etc. However, this can be effectively approximated by making products of the form  $(1 + v'_{\mathcal{C}}(\tau))$ , where  $\mathcal{C}$  is a cluster of the appropriate size. When such terms are distributed, one runs through possibilities of including or excluding each given cluster. This is only an approximation because the distribution will include extraneous terms in which we have clusters that overlap or are not far enough to be separate by the near neighbor approximation. In order to make the expansion systematic, we can correct for these extraneous cases at higher orders appropriately.

Let  $v_E^{(k)}(\tau)$  be the  $k^{\text{th}}$  order of our practical (more easily computable) cluster expansion, equivalent to the ideal cluster expansion (subsets composed of clusters up to size  $k$ ) up to  $k^{\text{th}}$  order. At the lowest order, we have

$$v_E^{(2)}(\tau) = \prod_{|\mathcal{C}_2|=2} (1 + v'_{\mathcal{C}_2}(\tau)), \quad (24)$$

producing all subsets composed of pairs along with some extraneous terms that must be corrected at higher orders. With some foresight, at the next order we will not only include 3-clusters [Fig. 4(a)], we will also correct for overlapping pairs [Fig. 4(b)], extraneous terms from  $v_E^{(2)}(\tau)$ . To relate this order with the previous order, we can equate  $v_E^{(2)}(\tau)$  infused with 3-clusters to  $v_E^{(3)}(\tau)$  infused with overlapping pairs:

$$v_E^{(2)}(\tau) \prod_{|\mathcal{C}_3|=3} (1 + v'_{\mathcal{C}_3}(\tau)) = \quad (25)$$

$$v_E^{(3)}(\tau) \prod_{|\mathcal{C}_3|=3} \prod_{\substack{\mathcal{A} \cup \mathcal{B}=\mathcal{C}_3, \\ |\mathcal{A}|=|\mathcal{B}|=2}} \sqrt{1 + v'_{\mathcal{A}}(\tau)v'_{\mathcal{B}}(\tau)}$$

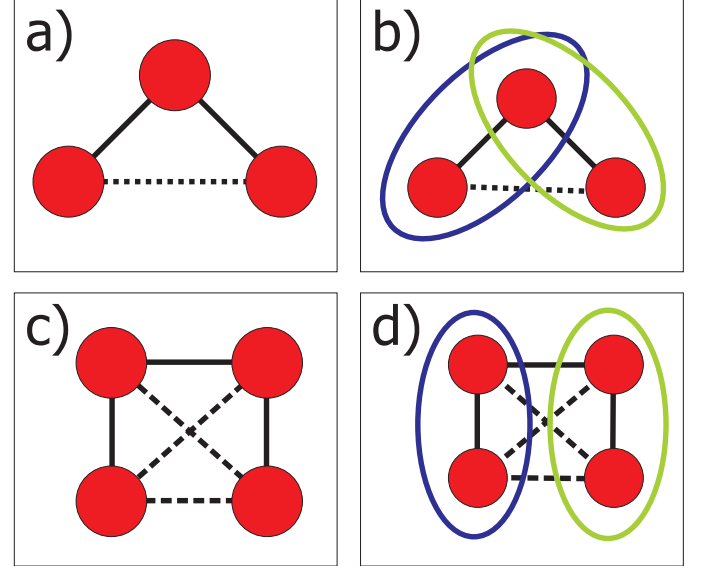


FIG. 4: Shown here are schematics of clusters that go into higher order corrections in the cluster expansion. Circles represent nuclei, solid lines represent pair-wise interactions between neighbors, dashed lines represent possible interactions between nuclei which may or may not be neighbors. a) and c) show 3-clusters and 4-clusters respectively. b) and d) show overlapping pairs and neighboring pairs respectively. The oval outlines in b) and d) envelope the different clusters (pairs) that are overlapping or neighboring.

The square root in Eq. (25) is necessary because  $\mathcal{A}$  and  $\mathcal{B}$  can be swapped in the product iterating over them; however, each factor may be combined with its counterpart (with  $\mathcal{A}$  and  $\mathcal{B}$  swapped) in order to remove the square root. It is therefore only a consequence of notation. This product, involving  $\mathcal{A}$  and  $\mathcal{B}$ , introduces overlapping pairs into  $v_E^{(3)}(\tau)$  so that we may relate it to  $v_E^{(2)}(\tau)$ . In this way,  $v_E^{(3)}(\tau)$  is defined in order to correct for the extraneous overlapping pairs of  $v_E^{(2)}(\tau)$ . This is not a perfect correction, however; it will generate more extraneous terms such as products of overlapping pairs with an embedded pair. These terms will be at least  $O(\lambda^6)$  since they involve a minimum of three pairs and therefore need only be corrected at higher orders of the expansion. Likewise, the added 3-clusters on the left hand side of Eq. (25) will generate extraneous terms to be corrected at higher orders. Therefore, consistent with the third order of the ideal cluster expansion (subsets composed of pairs and/or 3-clusters), we have, from Eq. (25),

$$v_E^{(3)}(\tau) = v_E^{(2)}(\tau) \prod_{|\mathcal{C}_3|=3} (1 + v'_{\mathcal{C}_3}(\tau)) \quad (26)$$

$$\times \prod_{\substack{|\mathcal{A} \cup \mathcal{B}|=\mathcal{C}_3, \\ |\mathcal{A}|=|\mathcal{B}|=2}} (1 + v'_{\mathcal{A}}(\tau)v'_{\mathcal{B}}(\tau))^{-1/2}.$$

Likewise,  $v_E^{(4)}(\tau)$  will introduce 4-clusters [Fig. 4(c)] and correct for neighboring pairs [Fig. 4(d)]. Consis-

tent with the fourth order of the ideal cluster expansion (subsets composed of pairs and/or 3-clusters and/or 4-clusters), we have

$$v_E^{(4)}(\tau) = v_E^{(3)}(\tau) \prod_{|\mathcal{C}_4|=4} (1 + v'_{\mathcal{C}_4}(\tau)) \times \prod_{\substack{|\mathcal{A} \cup \mathcal{B}|=\mathcal{C}_4, \\ |\mathcal{A}|=|\mathcal{B}|=2}} (1 + v'_{\mathcal{A}}(\tau)v'_{\mathcal{B}}(\tau))^{-1/2}. \quad (27)$$

As a general rule, convergence is such that,

$$v_E(\tau) = v_E^{(k)}(\tau)[1 + O(\lambda L)]. \quad (28)$$

This  $O(\lambda L)$  error is understood by realizing that, with an increase in size, cluster contributions increase by orders of  $\lambda$  and the cluster count increases by orders of  $L$ . Using these facts, we can write the following,

$$\prod_{|\mathcal{C}_k|=k} (1 + v'_{\mathcal{C}_k}(\tau)) \prod_{|\mathcal{C}_{k+1}|=k+1} (1 + v'_{\mathcal{C}_{k+1}}(\tau)) \quad (29)$$

$$= \prod_{|\mathcal{C}_k|=k} (1 + v'_{\mathcal{C}_k}(\tau))[1 + O(\lambda)v'_{\mathcal{C}_k}(\tau)]^L \quad (30)$$

$$= \prod_{|\mathcal{C}_k|=k} (1 + v'_{\mathcal{C}_k}(\tau))[1 + O(\lambda L)v'_{\mathcal{C}_k}(\tau)] \quad (31)$$

$$= \prod_{|\mathcal{C}_k|=k} (1 + v'_{\mathcal{C}_k}(\tau)[1 + O(\lambda L)]), \quad (32)$$

keeping only the lowest order of  $\lambda L$  and the lowest order in  $v'_{\mathcal{C}_k}(\tau) \sim O(\lambda^k)$ . In this treatment, we do not show the corrections for extraneous terms that, for example, show up in Eqs. (26) and (27). By design, however, corrections are made at the appropriate order of the expansion to be consistent with Eq. (28). Simply put, no correction may be relegated to a higher order if it impacts the current order.

Equation 28 assumes that  $v'_{\mathcal{C}_k}(\tau)$  with  $|\mathcal{C}_k| = k$  in general has a non-zero  $O(\lambda^k)$  term. It turns out, due to a symmetry of this problem, that there are no odd orders of  $\lambda$  contributing to the solution for either of the two perturbation expansions that we will associate with  $\lambda$ . This will be shown later for each of these perturbation expansions respectively. As a consequence,  $v_E^{(3)}(\tau)$  and  $v_E^{(4)}(\tau)$  are of the same order with regard to  $\lambda$ . In fact, if  $L > 1$ ,  $v_E^{(4)}(\tau)$  may introduce more significant corrections than those of  $v_E^{(3)}(\tau)$ . To be cautious, therefore, one must regard  $v_E^{(4)}(\tau)$ , not  $v_E^{(3)}(\tau)$ , to be the next order correction to  $v_E^{(2)}(\tau)$ .

It is useful, both in performing the calculations and to understand the effects of higher order corrections, to rewrite the above equations and formulas in an exponential form. Up to higher orders of  $\lambda$ , we can write  $(1 + v'_{\mathcal{C}}(\tau)) \approx \exp(v'_{\mathcal{C}}(\tau))$ . We may therefore approxi-

mate Eq. (24),

$$\ln(v_E^{(2)}(\tau)) \approx \Sigma_2(\tau), \quad (33)$$

$$\Sigma_2(\tau) = \sum_{|\mathcal{C}_2|=2} v'_{\mathcal{C}_2}(\tau). \quad (34)$$

This approximation is consistent with the second order of the cluster expansion. Using such a form [Eq. (33)] is convenient for performing the calculations (particularly for larger clusters) because it is straightforward to compute summations such as Eq. (34) via Monte-Carlo methods.

Similarly, for the next order of the expansion (fourth order in  $\lambda$ ), referring to Eqns. (26) and (27), we may write,

$$\ln(v_E^{(4)}(\tau)) \approx \ln(v_E^{(2)}(\tau)) + \Sigma_3(\tau) + \Sigma_4(\tau), \quad (35)$$

where

$$\Sigma_3(\tau) = \sum_{|\mathcal{C}_3|=3} \left( v'_{\mathcal{C}_3}(\tau) - \frac{1}{2} \sum_{\substack{\mathcal{A} \cup \mathcal{B}=\mathcal{C}_3, \\ |\mathcal{A}|=|\mathcal{B}|=2}} v'_{\mathcal{A}}(\tau)v'_{\mathcal{B}}(\tau) \right) \quad (36)$$

$$\Sigma_4(\tau) = \sum_{|\mathcal{C}_4|=4} \left( v'_{\mathcal{C}_4}(\tau) - \frac{1}{2} \sum_{\substack{\mathcal{A} \cup \mathcal{B}=\mathcal{C}_4, \\ |\mathcal{A}|=|\mathcal{B}|=2}} v'_{\mathcal{A}}(\tau)v'_{\mathcal{B}}(\tau) \right) \quad (37)$$

Equation (35) is consistent with the fourth order of the cluster expansion. This will not be correct to fourth order, however, if Eq. (33) is used to approximate  $\ln(v_E^{(2)}(\tau))$ . The appropriate fourth order variation of Eq. (33) is

$$\ln(v_E^{(2)}(\tau)) \approx \Sigma_2(\tau) + \Sigma_2^*(\tau), \quad (38)$$

$$\Sigma_2^*(\tau) = - \sum_{|\mathcal{C}_2|=2} (v'_{\mathcal{C}_2}(\tau))^2 / 2. \quad (39)$$

because  $(1 + v'_{\mathcal{C}}(\tau)) = \exp(v'_{\mathcal{C}}(\tau) - (v'_{\mathcal{C}}(\tau))^2/2) + O((v'_{\mathcal{C}}(\tau))^3)$ . Now we may write

$$\ln(v_E^{(4)}(\tau)) \approx \Sigma_2(\tau) + \Sigma_2^*(\tau) + \Sigma_3(\tau) + \Sigma_4(\tau), \quad (40)$$

consistent with the fourth order of the cluster expansion. We note that  $\Sigma_k \sim O(NL^{k-1}\lambda^k)$ , except that odd orders of  $\lambda$ , as we have discussed, will be skipped; also,  $\Sigma_2^* \sim O(NL\lambda^4)$ . With this in mind, this form [Eq. (40)], in addition to lending itself to Monte-Carlo techniques, is also helpful in understanding convergence. We further note that it is of practical importance that we combine the  $k$ -cluster contributions with corresponding corrections as is done in Eqs. (36) and (37) (i.e. combining each 4-cluster with corrections to neighboring pairs that

are embedded in the 4-cluster), because of the cancellations that take place. In fact,  $\Sigma_4(\tau)$  is only convergent, as one increases maximum neighbor distance, because of these cancellations.

For our purposes,  $v_E^{(2)}(\tau)$  will give a sufficient approximation to  $v_E(\tau)$ . Higher orders will only be calculated to estimate the error of this approximation and to compare the actual convergence for specific systems with the preceding theory. For the latter purpose, it will be useful to provide an order of magnitude estimate of  $v_E^{(5)}(\tau)$ . Without including all of the corrections (and corrections to previous corrections), we will use

$$\ln(v_E^{(5)}(\tau)) \approx \ln(v_E^{(4)}(\tau)) + \Sigma_5(\tau), \quad (41)$$

$$\Sigma_5(\tau) \sim \sum_{|\mathcal{C}_5|=5} \left( v'_{\mathcal{C}_5}(\tau) - \sum_{\substack{\mathcal{A} \cup \mathcal{B} = \mathcal{C}_5, \\ |\mathcal{A}|=3, |\mathcal{B}|=2}} v'_{\mathcal{A}}(\tau) v'_{\mathcal{B}}(\tau) \right). \quad (42)$$

It is necessary to subtract out embedded 2-cluster and 3-cluster combinations in order to achieve convergence as one increases maximum neighbor distance (similar to the situation with  $\Sigma_4(\tau)$ ). Unlike Eqs. (36) and (37) no factor of  $1/2$  is needed because  $\mathcal{A}$  and  $\mathcal{B}$  are defined to be different sizes and therefore can not be swapped. Again, Eq. (42) is only used to obtain an order of magnitude estimate of the fifth order correction to test this theory. Otherwise, many more corrections would have to be included.

## V. DUAL PERTURBATION THEORIES

The cluster expansion method explained in section IV requires an underlying perturbation theory to justify the requirement that large clusters provide smaller contributions (by orders of some perturbation parameter,  $\lambda$ ) than smaller clusters, which is the fundamental basis of the cluster expansion. In this section we will present two perturbation theories that are appropriate in opposing regimes. Both will require that  $\tau \ll \text{Max}(b_{nm})^{-1}$ . However, in problems we have considered  $\tau_D \ll \text{Max}(b_{nm})^{-1}$  where  $\tau_D$  is the decay time, and therefore this constraint has no practical consequence. These considerations make explicit the precise role and the definition of the perturbation expansion parameter  $\lambda$ , which has been a formal tool so far.

The first perturbation theory we will present is an expansion in orders of  $\tau$ . In relating this to the cluster expansion we can assign  $\lambda = \text{Max}(b_{nm})\tau$  (giving the origin of the constraint on  $\tau$  mentioned in the previous paragraph). We will see that this is convergent in the regime in which  $|A_n - A_m| \ll b_{nm}$ . Later, when we make a comparison between a strict application of the  $\tau$ -expansion and the cluster expansion, one has to keep in mind that,

for small enough  $\tau$ , there is convergence even when this criterion is not met.

The second perturbation theory, which we call the dipolar perturbation technique, will treat  $\mathcal{H}_B$  of Eq. (7) as a perturbation. Here,  $\lambda \sim b_{nm}/|A_n - A_m|$  in relating to the cluster expansion. This theory is therefore convergent in the opposite regime as the  $\tau$ -expansion with respect to  $|A_n - A_m|$  versus  $b_{nm}$ .

For convenience, we define,

$$c_{nm} = \frac{A_n - A_m}{4b_{nm}}, \quad (43)$$

so that the  $\tau$ -expansion perturbation theory is said to be applicable in the  $c_{nm} \ll 1$  regime while the dipolar perturbation is applicable in the  $c_{nm} \gg 1$  regime. The factor of 4 in Eq. (43) really only makes sense in the context of spin-1/2 nuclei, but it is irrelevant in distinguishing the two regimes.

These complementary perturbation theories are only used to justify the cluster expansion. If the cluster expansion uses exact results for cluster contributions, then either regime is justified per cluster. Therefore one can have a mixture of  $c_{nm} \ll 1$  clusters and  $c_{nm} \gg 1$  clusters as long as the  $c_{nm} \sim 1$  clusters are rare enough not to affect the result. We emphasize that our results are obtained from the full cluster expansion with the dual perturbation theory serving only as theoretical justification for its convergence and as independent checks on the result.

### A. Expansion in Tau

The first (but perhaps less relevant) perturbative expansion we will consider is an expansion of  $v_E(\tau)$  in orders of  $\tau$ . We will describe our initial attempt to apply this expansion directly, with results that are not useful for this problem, and later explain how this can be related to our more successful cluster expansion.

Our first attempt to obtain an estimated calculation of Eq. (18) for a large number of nuclei was to use computer algebra to expand it in powers of  $\tau$ . This is done by expanding the exponentials of  $U_{\pm}(\tau)$  [Eq. 16] in Eq. (18) and collecting all distributed terms of the desired order in  $\tau$ . One can additionally expand  $e^{-\mathcal{H}_n/k_B T}$ , from Eq. (15), in powers of  $T^{-1}$  but in the remaining discussion we will be taking the  $T \rightarrow \infty$  limit. It turns out that an expansion in  $\tau$  is not well suited for this problem because the time scale of the  $\tau$  expansion is affected by the values of  $A_n^{-1}$  which are typically much shorter than the decay time for many nuclei near the center of the electron wave function in a typical spectral diffusion problem. This discrepancy in time scales can be traced to the fact that  $|A_n - A_m| \gg \text{Max}(b_{nm})$  for many nuclear pairs in typical problems. This is the motivation for the perturbation expansion discussed in section V B. Although it is not well suited to this problem, we will discuss our

methods for performing this expansion and related calculations because it gives insight into the problem, and we will use it for comparison to the cluster method later. In addition, the  $\tau$ -expansion strategies described below may be adapted to other problems for which they are more suitable.

### 1. Algebraic Expansion

We developed a symbolic manipulation computer program that gives an exact algebraic expansion for any expansion order (although computation time limits the expansions that are feasible). The program uses its own algebraic manipulation library created precisely for this purpose and gives coefficients as reduced fractions rather than floating point numbers. This section describes the procedure used by the program.

For a particular order of  $\tau$ , an expansion of the exponentials will result in the trace of a sum of products of  $\mathcal{H}_\pm$ , and  $\mathcal{H}_B$ . The  $\mathcal{H}_\pm$  factors [Eq. (17)] can all be distributed to yield a sum of traces of products of  $\mathcal{H}_B$ , and  $\mathcal{H}_{An} = \frac{1}{2} \sum_n A_n I_{nz}$ . Each one of the Hamiltonian pieces,  $\mathcal{H}_{An}$ , and  $\mathcal{H}_B$ , involves sums over nuclear site indices. We can decrease the number of independent indices by one (not a major improvement, but enough to push this method one step further) by noting that

$$[\mathcal{H}_B, \mathcal{H}_{An}] = \frac{1}{2} \sum_{n \neq m} b_{nm} (A_n - A_m) I_{n-} I_{m+}, \quad (44)$$

which takes away the independence of  $\mathcal{H}_{An}$ 's index. Let  $\mathcal{H}_C = [\mathcal{H}_B, \mathcal{H}_{An}]$ . We can convert our sum of traced products of  $\mathcal{H}_{An}$  and  $\mathcal{H}_B$  into a sum of traced products of  $\mathcal{H}_{An}$  and  $\mathcal{H}_B$  and a single  $\mathcal{H}_C$  with one less independent summation index. The rest of this paragraph will briefly explain how this is done. Consider all of the terms that involve a certain number of  $\mathcal{H}_B$ 's, and  $\mathcal{H}_{An}$ 's. For any term, we can permute the  $\mathcal{H}_{An}$ 's and  $\mathcal{H}_B$ 's however we want at the expense of creating terms in which an  $\mathcal{H}_B \mathcal{H}_{An}$  combination is replaced by  $\mathcal{H}_C$  (which is the type of term we want anyway). Consider the set of terms that all have a certain number of  $\mathcal{H}_{An}$  factors and a certain number of  $\mathcal{H}_B$  factors. As long as the coefficients of such a set add up to zero, we can make the permutations cancel out, leaving only the terms with  $\mathcal{H}_C$  and one less independent summation index. By the symmetry in  $e^{\pm i \mathcal{H}_\pm \tau}$  of Eqs. (18) and (16), these coefficients add up to zero for all such sets in any order of  $\tau$ .

Consider pulling the summations over nuclear site indices, not only outside of each product, but also outside of the trace (since the trace of a sum is equal to the sum of the traces). The trace of these spin operators involving particular nuclear sites is straightforward to compute. In fact, all one really needs to know to perform the trace is which indices are the same and which ones are different (as well as the magnitude of the nuclear spins). Then one

can compute the trace as follows. If  $O_n$  is some operator (a product of spin operators  $I_{nz}$ ,  $I_{n+}$ ,  $I_{n-}$ ) that operates on the spin of site  $n$ , then

$$\frac{1}{M} \text{Tr}(O_1 O_2 \dots O_k) = \frac{\text{Tr}(O_1)}{M_1} \frac{\text{Tr}(O_2)}{M_2} \dots \frac{\text{Tr}(O_k)}{M_k}, \quad (45)$$

where  $M_n$  is the number of states of the  $n^{\text{th}}$  spin. To compute  $\text{Tr}(O_n) = \sum_i \langle i | O_n | i \rangle$  we simply use

$$I_\pm |I, m\rangle = \sqrt{I(I+1) - m(m \pm 1)} |I, m \pm 1\rangle, \quad (46)$$

$$I_z |I, m\rangle = m |I, m\rangle. \quad (47)$$

Of course, in order to obtain an algebraic expression for a particular order of  $\tau$ , we do not want to consider the sum of all possible nuclear site indices. In fact, in order to obtain this expression, we should not even need to know how many nuclear spins there are. Instead, we simply consider all of the possible “index configurations”. An “index configuration” indicates which indices are the same and which are different. As indicated above, this is enough information to allow one to evaluate the trace of the product of spin operators as a rational number (the square roots in Eq. (46) will always be repeated as factors an even number of times in the trace). Additionally, we need only consider “index configurations” that do not obviously result in a zero trace for any of the indices. In particular, we only need to consider configurations in which there are the same number of  $I_+$  as  $I_-$  operators for each index, and we can ignore any configuration in which the only operator for any index is an odd power of  $I_z$ .

Once the operators and traces are taken care of and we have exhausted all “index configurations,” we are left with terms that have factors of  $A_n$ 's and  $b_{nm}$ 's, some with the same nuclear index labels, and some with different labels. These labels are to be summed over distinctly (i.e. different labels should never be assigned the same index). The labels are arbitrary, so when checking for “like” terms, in order to provide a compact expression for the result, we should consider that the labels can be permuted. It would be a waste of computation time to always run through all permutations of labels when checking to see if two terms are like terms. Instead, the problem is transformed into that of checking for graph isomorphisms, which is a well-studied computational problem. The program uses a code called Nauty written by Brendan McKay (<http://cs.anu.edu.au/people/bdm>) for checking for graph isomorphisms.

The  $A_n$  and  $b_{nm}$  factors are transformed into a graph in the following way. Each distinct label is represented by a vertex in the graph. A factor of  $A_i^p$  is represented by coloring the vertex  $i$  to indicate the power  $p$ . A factor of  $b_{ij}$  is represented by an edge from vertex  $i$  to vertex  $j$ . If  $b_{ij}$  is raised to some power (other than 1) then it is represented by making an edge from both  $i$  and  $j$  to some special vertex that is colored in such a way as to indicate that it represents the appropriate power of  $b_{ij}$  (this is just a trick to effectively “color” edges). Then

the Nauty program takes this graph and gives a canonical labelling for the vertices. If the program comes to another term of  $A_n$  and  $b_{nm}$  factors that are equivalent to this one up to a permutation of labels, Nauty will give it the same canonical labelling so that the two terms can be combined.

The computer program's results for  $I = 1/2$  were compared to direct hand calculations (as a check) for up to 6<sup>th</sup> order in  $\tau$ . Actually, odd orders can be shown to be zero since the result must be real and  $\tau$  is always accompanied by a factor of  $i$ . The result is more compact when put in terms of  $c_{nm}$  as defined by Eq. (43). In this form the result is,

$$v_E(\tau) = 1 - D_4\tau^4 - D_6\tau^6 + O(\tau^8), \quad (48)$$

$$D_4 = 4c_{nm}^2 b_{nm}^4, \quad (49)$$

$$\begin{aligned} -\frac{3}{4}D_6 = & c_{nm}^4 b_{nm}^6 + c_{nm}^2 b_{nm}^6 \\ & + c_{nm}^2 b_{nm}^4 (b_{nk} - b_{mk})^2 \\ & + c_{nm} c_{nk} b_{nm}^2 b_{nk}^2 [b_{nk} (b_{nm} + b_{mk}) + b_{mk}^2], \end{aligned} \quad (50)$$

where distinct summation over indices is implied for each term. Written in this form (which is not the actual form given as output by our program), we can surmise that the  $\tau$  expansion gives convergence for  $\text{Max}(b_{nm})\tau \ll 1$  in the regime in which most pairs satisfy  $c_{nm} \ll 1$ . As indicated above, typical spectral diffusion problems have many pairs that satisfy  $c_{nm} \gg 1$  instead.

This program has computed algebraic expressions up to  $O(\tau^{10})$  for both  $I = 1/2$  and  $I = 3/2$ . In the  $I = 1/2$  case, there are 111 eighth order terms, and 1200 tenth order terms. Terms of order  $\tau^8$  have up to 4 distinct nuclear index labels; terms of order  $\tau^{10}$  have up to 5 distinct nuclear index labels. The trend that the number of distinct nuclear indices is half the order of  $\tau$  will be used in section V A 2 to relate the tau expansion to the cluster expansion.

After computing these algebraic expressions, there is an additional challenge of efficiently computing the coefficients of  $\tau$  from these expressions for specific values of  $A_n$  and  $b_{nm}$ . This is described in Appendix C.

## 2. Relating the Tau-Expansion to Clusters

The trend seen above is that the maximum number of distinct nuclear index labels is half of the order of  $\tau$ . This provides a connection to the cluster expansion. By definition, a cluster contribution gives just the terms of the solution that involve only and all of the nuclei in that cluster. The number of distinct nuclear indices for a cluster contribution is thus equal to the cluster size. Therefore, clusters of size 2 are, at a minimum, fourth order in  $\tau$ ; clusters of size 3 are  $O(\tau^6)$ , etc. Even if we cannot prove that this trend continues beyond  $O(\tau^{10})$  we know that clusters of size greater or equal to 5 are at least  $O(\tau^{10})$ . This is a key formal connection between the  $\tau$ -expansion and the cluster expansion.

We can therefore relate orders of  $\lambda$  used in section IV to orders of  $\tau$  (up to 5-clusters at least). As long as the  $\tau$  expansion is convergent for small  $N$ , the cluster expansion can be used to provide convergence for large  $N$ . As discussed above, this convergence in  $\tau$  occurs for  $\text{Max}(b_{nm})\tau \ll 1$  in the regime in which most pairs satisfy  $c_{nm} \ll 1$ . We also saw, from the argument that  $v_E(\tau)$  must be real, that no odd orders of  $\tau$  are present. Therefore, as discussed in section IV, the next order of the cluster expansion beyond pairs should include 3-clusters, 4-clusters and corrections to overlapping and neighboring pairs.

## B. Dipolar Perturbation Expansion

As mentioned in the beginning of section V A, an expansion in  $\tau$  is not well suited to practical problems of interest due to the many nuclear pairs satisfying  $c_{nm} \gg 1$ , as given in Eq. (43). However, in the regime in which  $c_{nm} \gg 1$ , a non-degenerate perturbation expansion in orders of  $b_{nm}$  is applicable. We introduce a bookkeeping parameter  $\lambda$  (which we will later relate to the  $\lambda$  used in section IV, making a formal connection to the cluster expansion) such that  $\pm \mathcal{H}_\pm = \mathcal{H}_0 \pm \lambda \mathcal{H}'$ . Here the unperturbed Hamiltonian  $\mathcal{H}_0 = \frac{1}{2} \sum_n A_n I_{nz}$  is diagonal in the nuclear spin  $z$ -basis, while  $\mathcal{H}' = \frac{1}{\lambda} \mathcal{H}_B$  is the dipolar interaction rescaled to have the same magnitude as  $\mathcal{H}_0$ . A convenient choice is to assume  $\lambda \sim 1/|c_{nm}| \sim \text{Max}(b_{nm})/\text{Max}(A_n) \sim 10^{-3}$ . We note that  $\lambda$  here is a purely formal artifice to define a perturbation expansion using standard perturbation theory in quantum mechanics (and later adapted to the cluster expansion of section IV in order to ensure convergence for large systems). In real calculations, one must ensure that the results converge as one goes to higher orders in  $\lambda$ , and the accuracy of the calculated results can only be ascertained by going to higher orders in  $\lambda$  and finding them to be small (as we explicitly do in our work).

### 1. Perturbation Theory

Using standard perturbation theory in quantum mechanics, we have the following recursive definitions for the eigenvectors and eigenvalues of  $\mathcal{H}_\pm$ :

$$|k_\pm\rangle = |k^0\rangle \pm \lambda \sum_{l \neq k} |l^0\rangle \times \quad (51)$$

$$\frac{\langle l^0 | \mathcal{H}' | k_\pm \rangle - \langle l^0 | k_\pm \rangle \langle k^0 | \mathcal{H}' | k_\pm \rangle}{E_k^{(0)} - E_l^{(0)}},$$

$$E_k^\pm = E_k^{(0)} \pm \lambda \langle k^0 | \mathcal{H}' | k_\pm \rangle, \quad (52)$$

$$E_k^{(0)} = \frac{1}{2} \sum_n A_n \langle k^0 | I_{nz} | k^0 \rangle \quad (53)$$

with the normalization convention that

$$\langle k^0 | k \rangle = \langle k^0 | k^0 \rangle = 1. \quad (54)$$

Now we have

$$\mathcal{H}_\pm = \pm \sum_k E_k^\pm \frac{|k_\pm\rangle \langle k_\pm|}{\langle k_\pm | k_\pm \rangle}, \quad (55)$$

where the summation is over all possible states. From Eq. (16),

$$U_\pm(\tau) = \sum_k \frac{|k_\pm\rangle \langle k_\pm|}{\langle k_\pm | k_\pm \rangle} e^{\mp i E_k^\pm \tau}. \quad (56)$$

Plugging this into Eq. (18), and taking the  $T \rightarrow \infty$  limit, we have,

$$v_E(\tau) = \sum_{i,j,k,l} \frac{C_{ijkl}}{M} \exp^{-i\omega_{ijkl}\tau}, \quad (57)$$

$$C_{ijkl} = \frac{F_{ijkl}}{D_{ijkl}}, \quad (58)$$

$$F_{ijkl} = \langle l_- | i_+ \rangle \langle i_+ | j_- \rangle \langle j_- | k_+ \rangle \langle k_+ | l_- \rangle, \quad (59)$$

$$D_{ijkl} = \langle i_+ | i_+ \rangle \langle j_- | j_- \rangle \langle k_+ | k_+ \rangle \langle l_- | l_- \rangle, \quad (60)$$

$$\omega_{ijkl} = \omega_{ijkl}^{(0)} + \lambda \omega'_{ijkl} \quad (61)$$

$$\omega_{ijkl}^{(0)} = E_i^0 - E_j^0 - E_k^0 + E_l^0 \quad (62)$$

$$\begin{aligned} \omega'_{ijkl} = & \langle i^0 | \mathcal{H}' | i_+ \rangle - \langle j^0 | \mathcal{H}' | j_- \rangle \\ & - \langle k^0 | \mathcal{H}' | k_+ \rangle + \langle l^0 | \mathcal{H}' | l_- \rangle. \end{aligned} \quad (63)$$

We note that  $C_{ijkl}$  and  $\omega'_{ijkl}$  can be expanded in orders of  $\lambda \sim c_{nm}^{-1}$ .

## 2. Relating the Dipolar Perturbation Expansion to Clusters

In order to use this dipolar perturbation expansion to validate the cluster expansion, we need to show that for a given term in the  $\lambda$  expansion of Eq. (57), there are at least as many orders of  $\lambda$  as there are nuclei involved (cluster size). We will show this to be effectively the case in the  $\text{Max}(b_{nm})\tau \ll 1$  limit. If we let  $\tau_D$  be the decay time, then the cluster expansion is justified by the dipolar perturbation for the full decay as long as  $\text{Max}(b_{nm})\tau_D \ll 1$ . This has indeed been the case for the spectral diffusion problems studied in this work.

First, let us only consider the nuclei involved in a term of  $F_{ijkl}$  (the numerator of  $C_{ijkl}$ ). The way in which nuclei “get involved” in  $F_{ijkl}$  is via the sum over nuclear pairs in  $\mathcal{H}' = \frac{1}{\lambda} \mathcal{H}_B$ . This gives potentially two nuclei for one  $\lambda$ , but we need to do better than that. Substituting  $|k_\pm\rangle$  on the right hand side of the Eq. (51) with the full expression will give successive orders of  $\lambda$ . When one considers a particular term of  $\langle l^0 | k_\pm \rangle$  with the above recursion formula in mind, one will go from state  $|l^0\rangle$  to state  $|k^0\rangle$  with some number of intermediate  $\mathcal{H}_0$  eigenstates in between where each state is connected to the

next via  $\mathcal{H}'$ . The second term in the numerator of Eq. (51) simply corresponds to going from state  $|l^0\rangle$  to  $|k^0\rangle$  through some number of intermediate states and then from  $|k^0\rangle$  back to  $|l^0\rangle$  through some more intermediate states. The point is simply that one goes from one state to a different state only via  $\mathcal{H}'$  [Eq. 17]. With this in mind, Eq. (59) indicates that one must go from state  $|i^0\rangle$  to  $|j^0\rangle$  to  $|k^0\rangle$  to  $|l^0\rangle$  and back to state  $|i^0\rangle$  with some number of states in between where consecutive states are connected via  $\mathcal{H}'$ . Because we must come back to state  $|i^0\rangle$ , for every lowering operator we pass through, we must also pass through a raising operator for the same spin. We now see that we can not actually get two nuclei for one  $\lambda$ ; for each nucleus involved in a given term of  $F_{ijkl}$ , there is at least one order of  $\lambda$ .

The denominator,  $D_{ijkl}$ , works in a similar way, except that instead of one cycle from state  $|i^0\rangle$  back to state  $|i^0\rangle$ , one has one of these going from  $|i^0\rangle$  to  $|i^0\rangle$ , another going from  $|j^0\rangle$  to  $|j^0\rangle$ , another going from  $|k^0\rangle$  to  $|k^0\rangle$ , and another going from  $|l^0\rangle$  to  $|l^0\rangle$ . But the result is the same; because these are all cyclic, there must be at least one order of  $\lambda$  for each nucleus involved. One then needs to perform the Taylor expansion of  $D_{ijkl}^{-1}$ . Let  $g(\lambda) = D_{ijkl}(\lambda)$  and  $f(\lambda) = \frac{1}{g(\lambda)}$ . The Taylor series expansion is,

$$f(\lambda) = \sum_{n=0}^{\infty} f^{(n)}(0) \frac{\lambda^n}{n!}, \quad (64)$$

where  $f^{(n)}(\lambda)$  may be obtained recursively with,

$$\left( \frac{g^{(m)}(\lambda)}{(g(\lambda))^k} \right)' = \frac{g^{(m+1)}(\lambda)}{(g(\lambda))^k} - k \frac{g^{(m)}(\lambda)}{(g(\lambda))^{k+1}}, \quad (65)$$

and then we note that  $(g(0))^k = 1$  so there will not be anything in the denominators of Eq. (65) to worry about in the context of Eq. (64). Examining the numerators in Eq. (65), we note that for each derivative of  $f(\lambda)$ , we will lose at most one order of  $\lambda$ . But in Eq. (64) for each derivative there is a factor of  $\lambda$  provided to compensate. If we write the  $\lambda$  expansion of  $g(\lambda)$  as

$$g(\lambda) = \sum_{n=0}^{\infty} g_n \lambda^n, \quad (66)$$

then, when we make the transformation to  $f(\lambda) = 1/g(\lambda)$ , each instance of  $g_n$  will be accompanied by at least  $n$  orders of  $\lambda$ . Therefore, after Taylor expanding the inverse of  $D_{ijkl}$ , we preserve the property that there are at least as many orders of  $\lambda$  as the number of nuclei involved in a given term.

We have dealt with the numerator and denominator of the amplitude, but we must still consider the frequency. We can rewrite the exponential in Eq. (57) as

$$e^{-i\omega_{ijkl}\tau} = e^{-i\omega_{ijkl}^{(0)}\tau} \exp(-i\lambda\omega'_{ijkl}\tau) \quad (67)$$

$$= e^{-i\omega_{ijkl}^{(0)}\tau} \sum_{n=0}^{\infty} \frac{(-i\lambda\omega'_{ijkl}\tau)^n}{n!}. \quad (68)$$

Thus we have transformed the perturbative part of the frequency into an amplitude (with a time dependence as well). We can now use a similar argument that was used for  $F_{ijkl}$  and  $D_{ijkl}$ . Each term of Eq. (63) will cycle from some state back to the same state with  $\mathcal{H}'$  connecting each intermediate state. As a result, there must be at least as many orders of  $\lambda$  in a given term of  $\lambda\omega'_{ijkl}$  as there are nuclei involved. There will, however, be one extra  $b_{nm}$ -type factor without an accompanying  $1/(A_n - A_m)$ . This gets combined with  $\tau$  and will be small as long as  $\text{Max}(b_{nm})\tau \ll 1$ . All of this can be exponentiated in the series of Eq. (68), but that can only increase orders of  $\lambda$  without increasing the number of nuclei involved.

There is one final consideration. How many nuclei are involved in  $\exp(-i\omega_{ijkl}^{(0)}\tau)$ ? From Eqs. (62) and (53), we see that this will include the nuclei that differ between states  $|i^0\rangle$  and  $|j^0\rangle$  along with the nuclei that differ between states  $|k^0\rangle$  and  $|l^0\rangle$ . Since a term of  $F_{ijkl}$  will require linking state  $|i^0\rangle$  to  $|j^0\rangle$  to  $|k^0\rangle$  to  $|l^0\rangle$  and back to  $|i^0\rangle$  via  $\mathcal{H}'$  (through some number of nuclear states), it must involve at least that many nuclei. So this factor will neither increase the number of involved nuclei nor change the number of  $\lambda$  factors.

We therefore conclude that, using an approximation that assumes  $\text{Max}(b_{nm})\tau \ll 1$ , there will be at least as many orders of  $\lambda$  in a term of the  $\lambda$ -expansion of Eq. (57) as there are nuclei involved. Therefore, a cluster contribution of size  $k$  will be of  $O(\lambda^k)$  or a higher order of  $\lambda$ . This justifies the cluster expansion in the regime in which  $c_{nm} \gg 1$  and  $\text{Max}(b_{nm})\tau \ll 1$ . To be more accurate and to relax the  $\text{Max}(b_{nm})\tau \ll 1$  constraint, as long as  $\text{Max}(b_{nm})\tau < 1$  we have shown that clusters of size  $k$  will give a contribution of order  $\lambda^{k-1}$ . Because it is consistent for different cluster sizes,  $k$ , and because clusters of size one do not contribute, this reduction by an order in  $\lambda$  does not have an impact upon the validity of the cluster expansion in any of its various forms (i.e. product form or exponentiated form). For simplicity of the discussion, however, we will regard  $\text{Max}(b_{nm})\tau$  simply as another order of  $\lambda$ .

One further point is that  $v_E(\tau)$  is an even function of  $\lambda$ . This is seen by noting that under the transformation  $\lambda \rightarrow -\lambda$  we have  $U_{\pm} \leftrightarrow U_{\mp}^{\dagger}$  and therefore,

$$v_E(\tau) = \frac{1}{M} \left| \text{Tr} \left\{ U_- U_+ U_-^{\dagger} U_+^{\dagger} \right\} \right| \quad (69)$$

$$\rightarrow \frac{1}{M} \left| \text{Tr} \left\{ U_+^{\dagger} U_-^{\dagger} U_+ U_- \right\} \right| = v_E(\tau). \quad (70)$$

This is true because there is a symmetry between “up” and “down”; that is,  $U_- \leftrightarrow U_+$  is symmetric within the trace operation because  $I_{nz} \rightarrow -I_{nz} \forall n$  is symmetric within the trace operation. A consideration of finite nuclear temperatures would break this symmetry, but in our infinite nuclear temperature approximation there will be no odd orders of  $\lambda$ . Therefore, as discussed in section IV, the next order of the cluster expansion beyond pairs

should include 3-clusters, 4-clusters and corrections to overlapping and neighboring pairs. This was shown to be necessary in section V A 2 when relating cluster sizes to orders of  $\tau$ , and it is also true here when relating cluster sizes to orders of the dipolar perturbation expansion.

## VI. CALCULATIONS AND RESULTS

The information (i.e. the input) necessary to calculate the spectral diffusion Hahn echo decay, given in Eq. (18) and approximated to lowest cluster expansion order with Eq. (24) or Eq. (33), are the  $A_n$ ,  $b_{nm}$ , and  $I_n$  (nuclear spin magnitude) values. For  $A_n$  and  $b_{nm}$ , repeating Eq. (8), we use,<sup>9</sup>

$$A_n = \frac{8\pi}{3} \gamma_S \gamma_I \hbar |\Psi(\mathbf{R}_n)|^2 \quad (71)$$

$$- \gamma_S \gamma_I \hbar \frac{1 - 3 \cos^2 \theta_n}{|\mathbf{R}_n|} \Theta(|\mathbf{R}_n| - r_0),$$

$$b_{nm} = -\frac{1}{4} \gamma_I^2 \hbar \frac{1 - 3 \cos^2 \theta_{nm}}{R_{nm}^3}. \quad (72)$$

Eq. (72) gives the dipolar coupling between a pair of nuclei where  $R_{nm}$  is their inter-nuclear distance and  $\theta_{nm}$  is their relative angle with respect to the magnetic field direction. The first term of Eq. (71) is the hyperfine coupling of the  $n$ th nucleus to the electron, while the second term is its dipolar coupling to the electron with  $r_0$  being the effective range of the wave function.  $\mathbf{R}_n$  is the position of the  $n$ th nucleus relative to the center of the electron wave function and  $\theta_n$  is its angle relative to this center, again, with respect to the magnetic field direction. While both of these terms were included in our calculations, the dipolar contribution of  $A_n$  proves to be negligible for the semiconductor spin quantum computer architectures.

### A. Phosphorus Donor in Silicon

Our first application is to consider the Hahn echo decay of the electron spin of a phosphorus donor in natural silicon.<sup>6,9,11</sup> Here  $\Psi(\mathbf{R}_n)$  is the Kohn-Luttinger wave function of a phosphorus donor impurity in silicon, as described in Ref. [9]. Using this in Eq. (71), we have,<sup>9</sup>

$$A_n = \frac{16\pi}{9} \gamma_S \gamma_I^{Si} \hbar \eta [F_1(\mathbf{R}_n) \cos(k_0 X_n) \quad (73)$$

$$+ F_3(\mathbf{R}_n) \cos(k_0 Y_n) + F_5(\mathbf{R}_n) \cos(k_0 Z_n)]^2$$

$$- \gamma_S \gamma_I^{Si} \hbar \frac{1 - 3 \cos^2 \theta_n}{|\mathbf{R}_n|} \Theta(|\mathbf{R}_n| - na),$$

$$F_{1,2}(\mathbf{r}) = \frac{\exp \left[ -\sqrt{\frac{x^2}{(nb)^2} + \frac{y^2+z^2}{(na)^2}} \right]}{\sqrt{\pi(na)^2(nb)}}, \quad (74)$$

with  $\gamma_S = 1.76 \times 10^7 (\text{s G})^{-1}$ ,  $\gamma_I^{Si} = 5.31 \times 10^3 (\text{s G})^{-1}$ ,  $n = 0.81$ ,  $a = 25.09 \text{ \AA}$ ,  $b = 14.43 \text{ \AA}$ ,  $\eta = 186$ ,

$k_0 = (0.85)2\pi/a_{Si}$ , and  $a_{Si} = 5.43$  Å. The Si nuclei are located on a diamond lattice.<sup>28</sup> The central <sup>31</sup>P nuclear spin does not contribute to spectral diffusion because its hyperfine energy is significantly larger than any of its neighbors, suppressing the spin flips by energy conservation. Finally, in a natural sample of silicon only a small fraction  $f = 4.67\%$  of lattice sites have non-zero nuclear spin. These are the spin-1/2 <sup>29</sup>Si isotopes, therefore  $I_n = 1/2$  for all contributing nuclei. Averaging Eq. (24) over all possible isotopic configurations gives

$$v_E(\tau) \approx \prod_{n < m} [1 + f^2 v'_{nm}(\tau)] \quad (75)$$

$$\approx \prod_{n < m} (1 + v'_{nm}(\tau))^{f^2}. \quad (76)$$

Or equivalently, averaging Eq. (33), we get

$$\ln(v_E(\tau)) \approx f^2 \Sigma_2^{(0)}(\tau), \quad (77)$$

where  $\Sigma_2^{(0)}(\tau) = \Sigma_2(\tau)/f^2$  is given by Eq. (34) when treating all nuclei as <sup>29</sup>Si. These are all equivalent approximations in the lowest order of the cluster expansion. Their equivalence requires that  $v'_{nm}(\tau) \sim O(\lambda^2) \ll 1$ , which, as we will show, is valid here to a high degree of accuracy. A more physical interpretation that  $v'_{nm}(\tau)$  should be effectively small is that spectral diffusion is a collective process caused by many nuclei so that each potentially flip-flopping nuclear pair contributes only a small amount to the overall dephasing before coherence is completely lost. Equations (75), (76), and (77) have all been used to compute results for Si:P with negligible difference between them.

For the spin-1/2 nuclei that contribute to spectral diffusion in natural silicon, we can write the following analytical solution for pairs (2-clusters) using Eq. (18),

$$v_{nm}(\tau) = 1 + v'_{nm}(\tau) = 1 - \frac{c_{nm}^2}{(1 + c_{nm}^2)^2} [\cos(\omega_{nm}\tau) - 1]^2, \quad (78)$$

$$\omega_{nm} = 2b_{nm}\sqrt{1 + c_{nm}^2}. \quad (79)$$

We repeat our definition of  $c_{nm}$ ,

$$c_{nm} = \frac{A_n - A_m}{4b_{nm}}. \quad (80)$$

Our numerical calculations of Hahn echo decay, using Eqs. (76) and (78), for several magnetic field orientation angles are shown on Fig. 5(a) with a direct quantitative comparison to the experiment<sup>10</sup>. Equation (72) contains an important anisotropy with respect to the angle  $\theta_{nm}$  formed between the applied magnetic field and the bond vector linking the two spins ( $\mathbf{R}_{nm}$ ). This property leads to a strong dependence of spin echo decay when the sample is rotated with respect to the applied B field direction. The experimental data is taken for bulk natural silicon with phosphorus doping concentration equal to

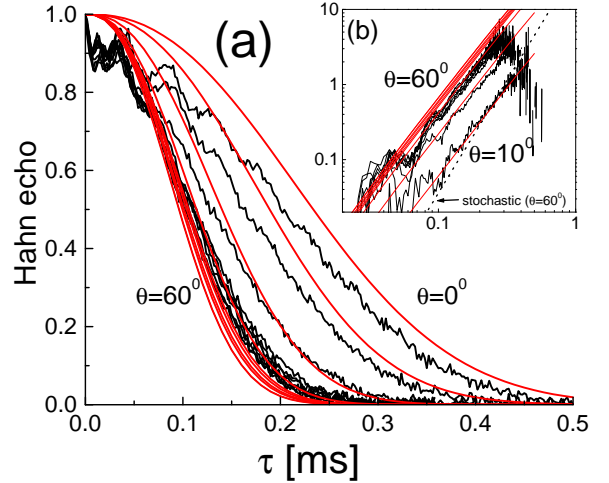


FIG. 5: Hahn echo decay  $v_E(\tau, \theta)$  of a phosphorus donor electron spin in silicon due to the dipolar nuclear spin bath dynamics. (a) Theory (solid lines) and experiment<sup>10</sup> is shown for several orientation angles of the magnetic field with respect to the crystal lattice, ranging from the [100] to the [110] direction ( $\theta = 0, 10, 20, \dots, 90$ ). (b) Here we plot  $-\ln v_E(\tau, \theta) + \ln v_E(\tau, \theta = 0)$ , allowing for the removal of any decoherence mechanism which is independent of  $\theta$ . The qualitative and quantitative agreement between theory and experiment is remarkable, in contrast to the stochastic approach (dashed).

$2 \times 10^{15}$  cm<sup>3</sup> [10]. The high concentration of phosphorus donors leads to an additional decoherence channel arising from the direct spin-spin coupling between the electron spins that contribute to the echo. This contribution can be shown to add a multiplicative factor  $\exp(-\tau/1\text{ ms})$  to Eq. (76).<sup>29</sup> Because this contribution is independent of the orientation angle, we can factor it out by subtracting the  $\theta = 0$  contribution from the logarithm of the experimental data taken at angle  $\theta$ . The result is shown on Fig. 5(b) (log-log scale). Our theory seems to explain the time dependence of the experimentally observed echo quite well. This result is to be compared with the recent stochastic theory of Ref. [9] (Dashed line in Fig. 5(b) shows the stochastic calculation for  $\theta = 60^\circ$ ). Although the stochastic theory yields the correct order of magnitude for the coherence times, it fails qualitatively in explaining the time dependence (that is, the shape of the decay as can be seen from the incorrect slope of the stochastic calculation in the log-log plot of Fig. 5(b)). The present method is able to incorporate all these features within a fully microscopic framework, obtaining both qualitative and quantitative agreement with experiment.

An important issue in the context of quantum information processing is the behavior of spin coherence at the shortest time scales. The experimental data<sup>10</sup> in Fig. 5 reveals several oscillatory features which are not explained by our current method. These are echo modulations arising from the anisotropic hyperfine coupling

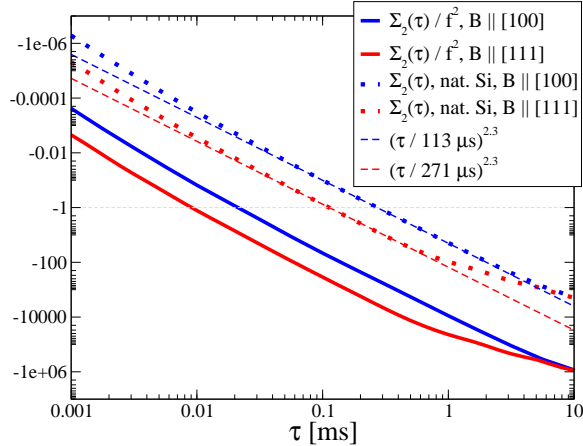


FIG. 6: Lowest order results for the natural log of the Hahn echo,  $\ln(v_E(\tau)) \approx \Sigma_2(\tau) = f^2 \Sigma_2^{(0)}(\tau)$ , for Si:P in a log-log plot. The  $y$ -axis is negative and inverted. The solid lines give  $\Sigma_2^{(0)}(\tau) = \Sigma_2(\tau)/f^2$ , which is independent of the  $^{29}\text{Si}$  fraction,  $f$ . Dotted lines give  $\Sigma_2(\tau) = f^2 \Sigma_2^{(0)}(\tau)$  for natural Si ( $f = 4.67\%$ ). In this log-log plot, multiplying by  $f^2$  simply shifts the curves vertically. Isotopic purification would shift these curves up further. The two magnetic field angles shown give extremal results. Corresponding to  $\theta$  angles in Fig. 5,  $B \parallel [100]$  is  $\theta = 0^\circ$  and  $B \parallel [111]$  is  $\theta \approx 54.7^\circ$ . Dashed lines fit these natural Si curves near their  $-1$  values (where  $v_E \sim 1/e$ ) with  $\tau^{2.3}$  power law curves (linear in the log-log plot).

omitted in Eq. (5).<sup>11</sup> This effect can be substantially reduced by going to higher magnetic fields. (In a quantum computer  $B \sim 9$  Tesla will probably be required in order to avoid loss of fidelity due to echo modulation.<sup>30</sup>) On the other hand, spectral diffusion itself is essentially independent of magnetic field even to extremely high magnetic field values ( $B \sim 10$  Tesla). The echo modulation effect is expected to be absent in III-V materials,<sup>31</sup> hence our theory allows the study of spin coherence at time scales of great importance for quantum information purposes, i.e. very short time scales, as long as echo modulation effects are quantitatively unimportant.

Isotopic purification can reduce the value of  $f$  (fraction of  $^{29}\text{Si}$  nuclei). Fig. 6 contains information that is useful for understanding how the Hahn echo curves change as  $f$  is changed (i.e. lowered via isotopic purification). In a log-log plot,  $\ln(v_E(\tau)) \approx \Sigma_2(\tau) = f^2 \Sigma_2^{(0)}(\tau)$  simply shifts vertically when  $f$  is changed. Fig. 6 shows both  $\Sigma_2(\tau)/f^2 = \Sigma_2^{(0)}(\tau)$ , independent of  $f$ , and  $\Sigma_2(\tau) = f^2 \Sigma_2^{(0)}(\tau)$  for natural Si ( $f \sim 5\%$ ). Results are shown for magnetic field angles that yield the extremal slowest and fastest decoherence. For natural Si, in a wide range of  $\tau$  about  $\tau_{1/e}$ , where  $v_E(\tau_{1/e}) = 1/e$ ,  $\Sigma_2(\tau)$  matches  $\tau^{2.3}$  curves very well. In this range of  $\tau$ , therefore, we may write,

$$v_E(\tau) \approx \exp(-f^2(\tau/\tau_0)^{2.3}), \quad (81)$$

$$= \exp(-(\tau/\tau_{1/e})^{2.3}), \quad (82)$$

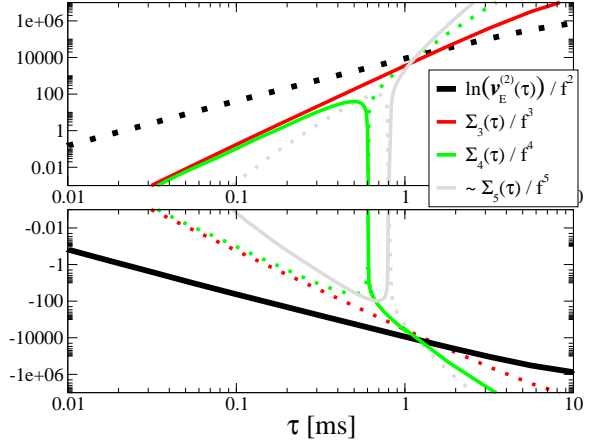


FIG. 7: Successive orders of the cluster expansion for the natural log of the Hahn echo [Eq. (84)], computed for Si:P and  $B \parallel [100]$ , with the dependence upon  $f$  divided out of each term. One can think of these curves as results for the 100%  $^{29}\text{Si}$  theoretical scenario. The thick black line gives the lowest order result, other solid lines give the indicated  $\Sigma(\tau)$  functions, and the dotted lines give the negative of their corresponding functions provided to assist in the absolute value comparison of these higher order corrections. As one would expect for  $L \sim 1$ , third and fourth orders [Eqs. (87) and (88)] are, at least initially, the same order of magnitude. As  $\tau$  increases, the effective value of  $L$ , average number of influential neighbors, increases. This causes higher orders to increase in absolute magnitude more quickly than smaller orders, all catching up together near  $\tau \sim 1$  ms.

where

$$\tau_{1/e} = \tau_0/f^{2/2.3}, \quad (83)$$

providing a formula that allows us to adjust our Hahn echo curves to other values of  $f$  for a range of  $\tau$  in which Eq. (81) is applicable.

We now check the convergence of our cluster expansion for this Si:P system. From Eqs. (35) and (41), we have

$$\begin{aligned} \ln(v_E(\tau)) \approx & \ln(v_E^{(2)}(\tau)) + \Sigma_3(\tau) \quad (84) \\ & + \Sigma_4(\tau) + \Sigma_5(\tau), \end{aligned}$$

valid to fourth order in the cluster expansion and with  $\Sigma_5(\tau)$  as defined by Eq. (42) giving only an order of magnitude estimate of the fifth order correction. Averaging over all possible isotopic configurations gives,

$$\Sigma_k(\tau) = f^k \Sigma_k^{(0)}(\tau), \quad (85)$$

where  $\Sigma_k^{(0)}(\tau) = \Sigma_k(\tau)/f^k$  is evaluated using Eqs. (36), (37), and (42) with all nuclear sites treated as  $^{29}\text{Si}$ . These  $\Sigma(\tau)$  functions have been calculated using Monte-Carlo techniques with cluster contributions,  $v'_C(\tau)$ , for larger clusters than pairs, calculated by numerically diagonalizing  $\mathcal{H}_\pm$  [Eq. (17)]. The maximum distance between neighbors and the maximum distance of nuclei to the center of the dot is increased for various Monte-Carlo runs

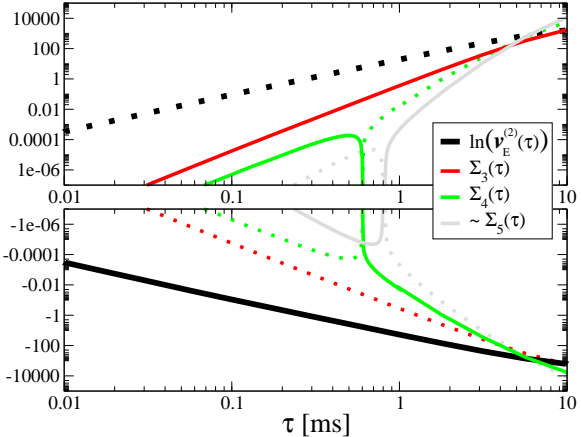


FIG. 8: Successive orders of the cluster expansion for the natural log of the Hahn echo,  $\ln(v_E(\tau))$ , computed for Si:P in natural Si ( $f = 0.0467\%$ ) with  $B \parallel [100]$ . The curves are the same as those in Fig. 7 except for vertical shifts (in this log-log plot) resulting from their respective dependence on  $f$ . Out to  $\tau = 1$  ms, where the Hahn echo has fully decayed beyond all practical purposes, the expansion is seen to converge very well; the contribution to  $\ln(v_E(\tau))$  is orders of magnitude smaller for each successive order of the cluster expansion. Near  $\tau \approx 10$  ms, the convergence fails. This reveals the limit of our expansion, but this limitation has no physical significance since it is well beyond the point of full decay for practical purposes.

until convergence within a desired precision is reached. To speed up each Monte-Carlo run, clusters are chosen with a heuristic bias for those that have strong coupling between the constituent nuclei as well as a bias for clusters close to the center of the quantum dot. Appropriate weighting factors are used to counteract these biases.

The terms of Eq. (84) scale with  $\lambda$ ,  $N$ , and  $L$  (average number of influential neighbors, proportional to  $f$ ) as follows,

$$\ln(v_E^{(2)}(\tau)) \sim O(NL\lambda^2), \quad (86)$$

$$\Sigma_3(\tau) \sim O(NL^2\lambda^4), \quad (87)$$

$$\Sigma_4(\tau) \sim O(NL^3\lambda^4), \quad (88)$$

$$\Sigma_5(\tau) \sim O(NL^4\lambda^5). \quad (89)$$

Fig. 7 compares  $\ln(v_E^{(2)}(\tau))/f^2$  to the higher order  $\Sigma_k^{(0)}(\tau)$  functions in a dual (showing positive and negative values) log-log plot for Si:P with  $B \parallel [100]$ . In other words, it compares successive order of the expansion for the natural log of the Hahn echo,  $\ln(v_E(\tau))$ , with the  $f$  dependence removed. As one might anticipate by the fact that  $\Sigma_3^{(0)}(\tau)$  and  $\Sigma_4^{(0)}(\tau)$  are both  $O(\lambda^4)$ , they are similar orders of magnitude, at least for the  $0.03 \text{ ms} < \tau < 1 \text{ ms}$  range. However, the effective value of  $L$  increases with  $\tau$  so that  $\Sigma_4^{(0)}(\tau)$  eventually surpasses  $\Sigma_3^{(0)}(\tau)$ . The physical explanation for this is that given enough time, more distant pairs will have an opportunity to flip-flop; there-

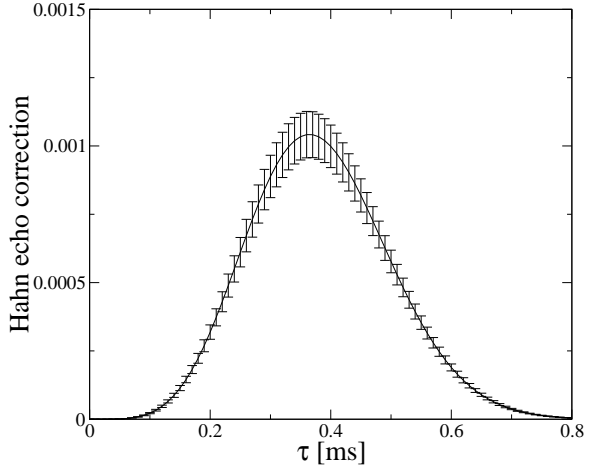


FIG. 9: The estimated correction to the lowest order Hahn echo decay for Si:P in natural silicon with  $B \parallel [100]$  due to higher orders of the cluster expansion. It is dominated by the third order of the cluster expansion and is therefore given by  $\exp(\Sigma_3(\tau))[v^{(2)}(\tau) - 1]$ . The error bars are a result of the standard deviation of the mean from our Monte-Carlo calculation of  $\Sigma_3(\tau)$ .

fore, the average number of influential neighbors will increase over time. Near  $\tau \sim 1$  ms all of these terms are roughly the same order of magnitude, corresponding to  $\lambda^2L \sim 1$ . At this point, the cluster expansion would break down for the  $f = 1$  case (which is only of theoretical interest). Fig. 8 compares the successive orders of the natural log of the Hahn echo [Eq. (84)] for natural Si,  $f = 0.0467$ . The log-log curves of Fig. 8 are the same as those of Fig. 7 with vertical shifts due to multiplying the terms of  $\ln(v_E(\tau))$  by appropriate powers of  $f$ . The higher orders have been shifted by a greater amount which has increased the separation between them. The convergence (observed by the separation between these orders) is good (with at least an order of magnitude separation between consecutive orders of the expansion) out to  $\tau \sim 1$  ms, well beyond the point in  $\tau$  that the Hahn echo has fully decayed for all practical purposes.

Fig. 9 shows the estimated correction to the lowest order solution due to higher orders for Si:P with natural Si and  $B \parallel [100]$ . It is apparent from Fig. 8 that this correction is dominated by the third order of the cluster expansion (3-clusters) and is therefore given by  $\exp(\Sigma_3(\tau))[v^{(2)}(\tau) - 1]$ . The absolute value of the higher order correction may be considered to be an approximation of the error of the lowest order result. At its maximum, this absolute error is approximately 0.001. Although our cluster expansion fails near  $\tau > 1$  ms, the absolute (as opposed to relative) error will stay small if we assume that our Hahn echo decay is forever monotonically decreasing. For all practical purposes, the lowest order result is therefore valid up to 0.1% of the original  $v_E(0) = 1$ , and higher order terms only provide corrections beyond 99.9% accuracy level.

We have also verified that our cluster expansion results

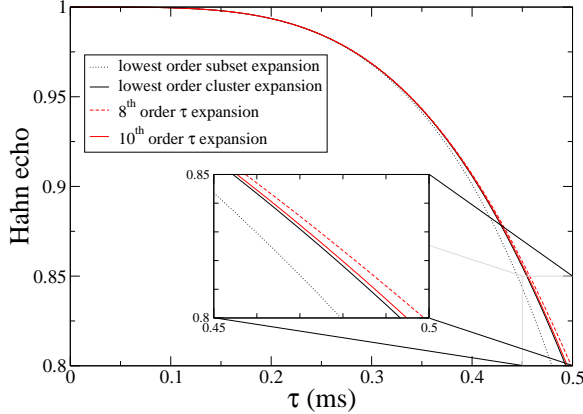


FIG. 10: This compares the  $\tau$ -expansion results with the lowest order cluster-expansion result [Eq. (24)] for an arbitrary set of nuclei (ranging from 15 to 20 lattice constants away from the center) for the phosphorus donor in natural silicon. Shown are the  $\tau$ -expansion results at the highest two orders of  $\tau$  that we have computed. Note the agreement with the cluster expansion results before the two  $\tau$ -expansion results diverge. Also shown is the lowest order subset expansion results [Eq. (23) with  $k_0 = 2$ ] which does not agree so well.

agree quantitatively with the  $\tau$ -expansion [Eq. (48)] up to 10<sup>th</sup> order in  $\tau$  when excluding nuclei close to the center of the electron wave function where  $c_{nm} \gg 1$ . An example is given in Fig. 10. One other thing to note about these cluster expansion calculations is the following. Although performing exact cluster contribution calculations effectively interpolates between dual perturbation theories, valid in opposite regimes with respect to  $c_{nm}$ , we have observed that only the dipolar perturbation, valid for  $c_{nm} \gg 1$ , is necessary for this problem. This can be shown by comparing calculations that use exact pair contributions versus approximate pair contributions in the lowest order of the dipolar perturbation. One must exclude pairs in which  $c_{nm} < 1$  since the dipolar perturbation diverges for small  $c_{nm}$ , but this cut-off point is flexible. The fact that there is no noticeable difference in these differently calculated decay curves is evidence that only  $c_{nm} \gg 1$  pairs contribute to spectral diffusion in this problem and therefore only dipolar perturbation is needed. Pairs in which  $c_{nm} < 1$  do not contribute because they operate on longer time scales than the decay time.

## B. Gallium Arsenide Quantum Dot

Next we consider the Hahn echo decay of a localized quantum dot electron spin in GaAs. For this,  $\Psi(\mathbf{R}_n)$  will be the quantum dot wave function parameterized by the quantum well thickness,  $z_0$ , and Fock-Darwin radius,  $\ell(B)$  (a function of the magnetic field strength), as de-

scribed in Ref. [9]. Using this in Eq. (71), we have,<sup>9</sup>

$$A_n = \frac{16}{3} \frac{\gamma_S \gamma_I \hbar (a_{GaAs}^3 / 4)}{\ell^2(B) z_0} d(I) \cos^2 \left( \frac{\pi}{z_0} Z_n \right) \quad (90)$$

$$\times \exp \left( -\frac{X_n^2 + Y_n^2}{\ell^2(B)} \right) \Theta(z_0/2 - |Z_n|)$$

$$- \gamma_S \gamma_I \hbar \frac{1 - 3 \cos^2 \theta_n}{|\mathbf{R}_n|^3} \Theta(X_n^2 + Y_n^2 - \ell^2(B)),$$

with  $a_{GaAs} = 5.65$  Å and  $\gamma_S = 1.76 \times 10^7$  (s G)<sup>-1</sup> (the free electron gyromagnetic ratio). The GaAs lattice has a Zincblende structure with two isotopes of Ga atoms placed on one fcc lattice and <sup>75</sup>As atoms placed on the other fcc lattice.<sup>28</sup> The Ga isotopes are 60.4% <sup>69</sup>Ga and 30.2% <sup>71</sup>Ga.<sup>9,32</sup> We used  $\gamma_I = 4.58, 8.16, 6.42 \times 10^3$  (s G)<sup>-1</sup> and  $d(I) = 9.8, 5.8, 5.8 \times 10^{25}$  cm<sup>-3</sup> for <sup>75</sup>As, <sup>71</sup>Ga, and <sup>69</sup>Ga respectively.<sup>9,33</sup> All of these nuclei have a valence spin of  $I = 3/2$  which means that Eq. (78) is not applicable. As with the higher order correction calculations section VIA, we obtain cluster contributions by diagonalizing  $\mathcal{H}_\pm$  numerically.

Most of our results only include dipolar interactions for  $b_{nm}$  [Eq. 72]. However, indirect exchange interactions<sup>15,16,17</sup> between the nuclei of GaAs may be of the same order of magnitude as the dipolar interactions [Eq. 72] between nearest neighbors.<sup>13</sup> There is enough quantitative ambiguity in the literature about the indirect exchange interaction that we have chosen to leave it out of our calculations in order to have a precise theory for the dipolar nuclear spin bath dynamics only. We make an exception near the end of this section where we make a comparison to the results in Ref. [13] that include this interaction.

With exception to the  $I_{nz} I_{mz}$  term in  $\mathcal{H}_B$  [Eq. (7)], the different types of nuclei are decoupled. In the lowest order of the cluster expansion, the different types of nuclei truly are decoupled because a pair cannot contribute to the spectral diffusion without the flip-flop interaction between them. Furthermore, this  $b_{nm} I_{nz} I_{mz}$  term is negligible where the dipolar perturbation is applicable because the diagonal of the Hamiltonian in the nuclear  $z$ -basis will be dominated by  $\mathcal{H}_A$ . We will later discuss comparisons made between calculations using exact pair contributions versus approximate pair contributions using the lowest order dipolar perturbation (also done in section VIA for Si:P) to demonstrate that the dipolar perturbation theory is applicable. Using these arguments, we will simplify our calculations by approximating Eq. (7) with

$$\mathcal{H}_B \approx \sum_{n \neq m} b_{nm} \delta(\gamma_n - \gamma_m) I_{n+} I_{m-}. \quad (91)$$

This approximation effectively decouples the As nuclei from the Ga nuclei and the Ga isotopes from each other. Although it is possible to perform our cluster calculations without this approximation (we have done so for some lowest order calculations with no additional complication and the difference is indeed negligible), it avoids

unnecessary complications for higher order calculations. We may then perform calculations for each of these separately using Eqs. (40) and (41). Using the subscript  $x$  to represent each of these types of nuclei, we have

$$\ln(v_E(\tau)) \approx \sum_x \{ f_x^2 \Sigma_{2x}(\tau) + f_x^2 \Sigma_{2x}^*(\tau) + f_x^3 \Sigma_{3x}(\tau) + f_x^4 \Sigma_{4x}(\tau) \}. \quad (92)$$

We compute  $\Sigma_{kx}(\tau)$  and  $\Sigma_{2x}^*(\tau)$  with Eqs.(34), (39), (36), (37), and (42) for an fcc lattice fully occupied by nuclei of type  $x$  using a Monte-Carlo technique as described below Eq. (85). For  $^{75}\text{As}$ ,  $^{71}\text{Ga}$ , and  $^{69}\text{Ga}$ , it is appropriate to use  $f_x = 100\%$ ,  $30.2\%$ , and  $60.4\%$  respectively. We now define  $\Sigma_k(\tau) = \sum_x f_x^k \Sigma_{kx}(\tau)$  and  $\Sigma_2^*(\tau) = \sum_x f_x^2 \Sigma_{2x}^*(\tau)$  so that we have

$$\ln(v_E(\tau)) \approx \Sigma_2(\tau) + \Sigma_2^*(\tau) + \Sigma_3(\tau) + \Sigma_4(\tau), \quad (93)$$

valid to fourth order in the cluster expansion.

The lowest order results,  $v_E(\tau) \approx \exp(\Sigma_2(\tau))$ , for most of our GaAs calculations show a Hahn echo decay of the form  $\exp(-(2\tau/t_0)^4)$ . This differs qualitatively from the decay for the Si:P which, by our calculations, is in the form  $\exp(-(2\tau/t_0)^\alpha)$  where  $\alpha \sim 2.3$  for a range of  $\tau$  appropriate for natural Si and some range of isotopic purification. The form of the GaAs echo decay does not change if we repeat the calculation with  $I = 1/2$  rather than  $3/2$ , although  $t_0$  does change. The qualitative difference between Si:P and GaAs dot solutions is therefore not due to the difference in spin magnitude of the nuclei, but rather the difference in the form of the electron wave function and lattice occupation leading to different distributions of  $c_{nm}$  values. GaAs, in ranges of tested  $z_0$  and  $\ell$  parameters, has a more narrow distribution of  $c_{nm}$  for significantly contributing pairs than that of the Si:P problem. As a result of this narrow distribution, the fact that the lowest non-trivial order of the  $\tau$ -expansion is  $O(\tau^4)$ , which is universal for all values of  $I$ , expresses itself in the sum of pair contributions in Eq. (34) for  $\Sigma_2(\tau)$ . This  $\exp(-(2\tau/t_0)^4)$  form is confirmed by Yao *et al*<sup>13</sup> using a completely different theoretical technique. Yao *et al* use a pair-correlation quasi-particle approach to the “spectral diffusion” problem that is equivalent to our lowest order cluster expansion, and they give results for quantum dots in GaAs. They come to the same conclusion that the form of the decay depends on the relative breadth of the excitation spectrum.

Figs. 11 and 12 show the  $t_0$  of the initial  $\exp(-(2\tau/t_0)^4)$  Hahn echo decay for various parameter settings of  $z_0$  and  $\ell$  with two different magnetic field orientations. Also shown is  $t_{1/e}$ , defined such that  $v_E(\tau = t_{1/e}/2) = e^{-1}$ . One can think of this  $t_{1/e}$  as an effective  $T_2$ -time for the problem although the echo decay is not a simple exponential. Except for small dots,  $t_0 = t_{1/e}$ , indicating that the decay has the form  $\exp(-(2\tau/t_0)^4)$ . Small dots deviate from this form, beginning to have longer  $t_{1/e}$  decay times than their initial

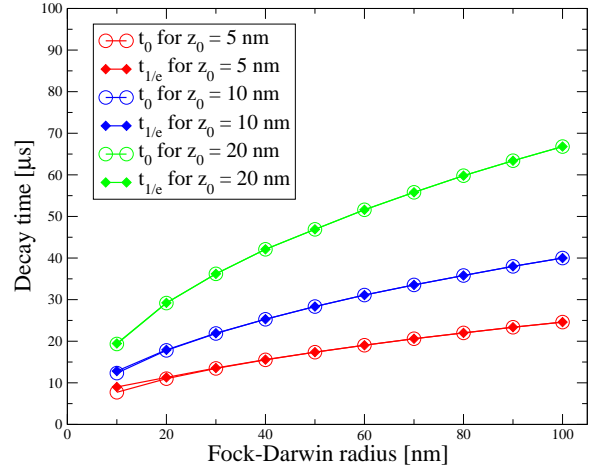


FIG. 11: For GaAs quantum dots, shows  $t_0$ , the characteristic initial decay time, and  $t_{1/e}$ , the  $e^{-1}$  decay time, versus the Fock-Darwin radius  $\ell$  for various quantum well thicknesses,  $z_0 = 5, 10, 20$  nm. The orientation of the magnetic field is parallel to [001] of the lattice; this is along the  $z_0$  confinement of the quantum dot.

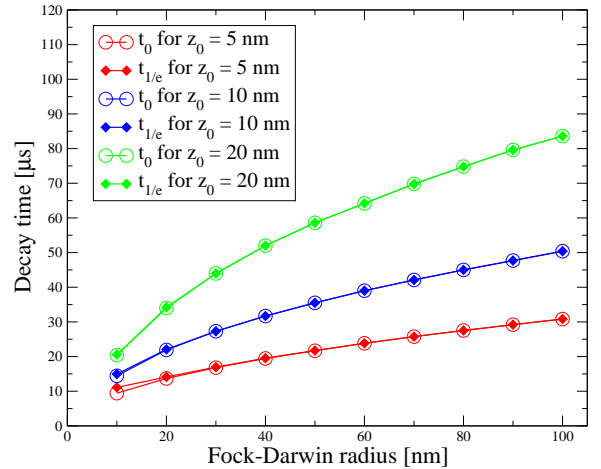


FIG. 12: For GaAs quantum dots, shows  $t_0$ , the characteristic initial decay time, and  $t_{1/e}$ , the  $e^{-1}$  decay time, versus the Fock-Darwin radius  $\ell$  for various quantum well thicknesses,  $z_0 = 5, 10, 20$  nm. The orientation of the magnetic field is parallel to [110] of the lattice; this is perpendicular to the  $z_0$  confinement of the quantum dot.

characteristic times,  $t_0$ . It was noted in Ref. [9] that decoherence times become infinite as the size of the quantum dot approaches zero or infinity with a minimum decoherence time at some finite size. The former is simply because the electron has no interaction with nuclei as the quantum dot size approaches zero, and the latter is because the nuclei all have the same coupling to the electron as the size becomes infinite. For  $z_0 = 5$  nm, we begin to approach this maximum decoherence (minimum  $t_{1/e}$ ) near  $\ell = 10$  nm, but only in the regime where  $t_{1/e}$  deviates from  $t_0$ .

As discussed previously, the Ga and the As nuclei, on

separate fcc lattices, are decoupled by our approximation [Eq. (91)]. In silicon, the asymmetry of the diamond lattice results in maximum decoherence in the [111] direction. In this case, because the fcc lattice is more symmetric, the angular dependence is primarily a result of the shape of the quantum dot (not the lattice). Figs. 11 and 12 show slight quantitative differences when the magnetic field is along the  $z_0$  confinement direction or perpendicular to it.

Because most of our GaAs results are in the form corresponding to the limit of small  $\tau$ , it is tempting to think that GaAs is dominated by the  $c_{nm} \ll 1$  regime appropriate for the  $\tau$ -expansion. However, as with the phosphorus donor in Si, we have compared calculations that use exact pair contributions versus approximate pair contributions using the lowest order dipolar perturbation. These different calculations agree very well for small quantum dots, but deviate slightly for larger quantum dots. Intermediate sized dots are well approximated by either perturbation theory. This is merely a result of small decoherence times such that the  $\tau$  approximation is valid even though most pairs have  $c_{nm} > 1$ . The agreement with the perturbation expansion gives justification for the approximation used in Eq. (91) in which  $b_{nm} I_{nz} I_{mz}$  was neglected.

We now return to a discussion of the indirect exchange interaction between nuclear spins (mediated by virtual interband electronic transitions) that were neglected in the above calculations. Including the exchange interaction, we should use

$$b_{nm} = b_{nm}^d + b_{nm}^e, \quad (94)$$

where  $b_{nm}^d$  is the dipolar coupling [Eq. 72], and  $b_{nm}^e$  is the indirect exchange coupling. We note that  $b_{nm}^e = 0$  in the Si:P system to a high degree of accuracy. Yao *et al*<sup>13</sup> performed spectral diffusion decoherence calculations (using an equation that is equivalent to our lowest order result) for GaAs quantum dots including the indirect exchange interaction. As a verification of the correctness of our calculations, Fig. 13 reproduces their Hahn echo results using our method but including the indirect exchange interactions as given by<sup>17</sup>

$$b_{nm}^e = -\gamma_n \gamma_m m \hbar \frac{\sqrt{2.6} \text{ \AA}}{2R_{nm}^4}. \quad (95)$$

There is ambiguity in the literature about the appropriate sign of Eq. (95). We have adopted the convention used by Yao *et al*<sup>13</sup> in order to reproduce their results. Fig. 13 also shows the results for the same parameters when the indirect exchange is excluded; it is apparent that this coupling is significant, at least in GaAs quantum dots for these choices of the exchange coupling. The kink in the  $t_{1/e}$  curve for the case of excluded indirect exchange is believed to be a discrete lattice effect only noticeable for small quantum dots. For such small quantum dots, it is likely that Eq. (90), derived from an approximate electron wave function, is somewhat inaccurate.

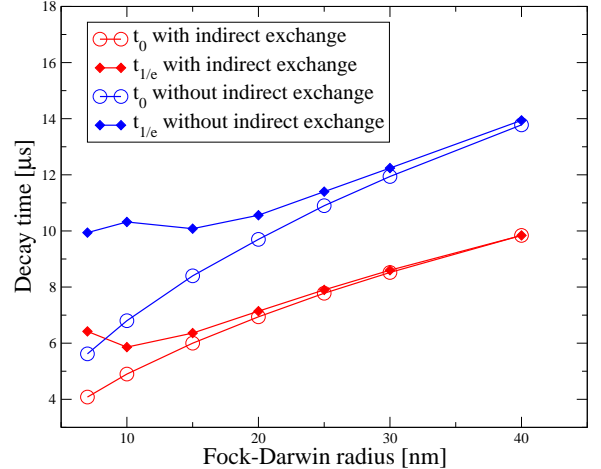


FIG. 13: For GaAs quantum dots, shows  $t_0$ , the characteristic initial decay time, and  $t_{1/e}$ , the  $e^{-1}$  decay time, versus the Fock-Darwin radius  $\ell$  for a quantum well thicknesses of  $z_0 = 2.8$  nm. The orientation of the magnetic field is parallel to [110] of the lattice; this is perpendicular to the  $z_0$  confinement of the quantum dot. This shows results both when including or excluding the indirect exchange coupling.

With our cluster expansion approach, we can estimate the error of our calculated decay curves by performing higher order calculations. We observe that the larger quantum dots have larger corrections. For quantum dots with  $z_0 = 20$  nm and  $\ell = 100$  nm our calculations indicate maximum correction to the Hahn echo decay curves on the order of  $10^{-3}$ , 0.1% of the initial  $v_E(0) = 1$ , just as it was for natural silicon [Fig. 9]. For dots with  $z_0 = 5$  nm and  $\ell = 10$  nm, absolute corrections are on the order of  $10^{-4}$ , 0.01% of the initial  $v_E(0) = 1$ . Fig. 14, analogous to Fig. 8, gives a dual (showing positive and negative values) log-log plot for the higher order contributions to the natural log of the Hahn echo [Eq. (93)] for an intermediate size ( $z_0 = 10$  nm,  $\ell = 50$  nm) GaAs quantum dot. Higher order corrections are clearly negligible out to  $\tau \sim 0.1$  ms, well beyond the point in which the Hahn echo has fully decayed for all practical purposes.

## VII. CONCLUSION

In conclusion, we describe a new quantum approach for the problem of localized electron spin decoherence due to the fluctuation of dipolar coupled nuclear spins. In contrast to former theories, our method requires no *ad hoc* stochastic assumption on the complex dynamics of the environment responsible for decoherence. Hence it provides an important example where direct integration of the environmental equations of motion provides a systematic understanding of the loss of coherence which needs to be controlled for quantum information applications.

The most important theoretical accomplishment of our

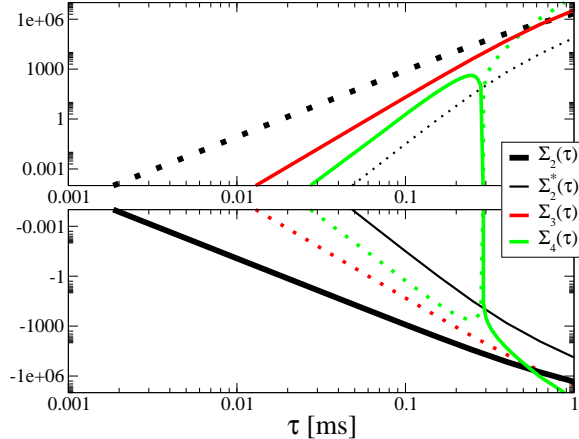


FIG. 14: Higher orders of the cluster expansion for the natural log of the Hahn echo [Eq. (93)], computed for a GaAs quantum dot with  $B \parallel [110]$ ,  $z_0 = 10$  nm, and  $\ell = 50$  nm. The thick black line gives the lowest order result, other solid lines give the indicated  $\Sigma(\tau)$  functions, and the dotted lines give the negative of their corresponding functions provided to assist in the absolute value comparison of these higher order corrections. This plot includes  $\Sigma_2^*(\tau)$  which estimates the error in approximating  $\ln(v_E^{(2)})$ , from Eq. (24), with  $\Sigma_2(\tau)$ , Eq. (33). This log-log plot demonstrates that all of the  $O(\lambda^4)$  corrections,  $\Sigma_2^*(\tau)$ ,  $\Sigma_3(\tau)$ , and  $\Sigma_4(\tau)$ , are negligible in the relevant range of  $\tau$  (before the Hahn echo has fully decayed in the lowest order,  $-\Sigma_2(\tau) \gg 1$ , for all practical purposes).

work is the development of the first *fully quantum microscopic* theory for the localized electron spin decoherence due to the spectral diffusion induced by nuclear spin bath dynamics. The important nuclear spin dynamics for the spectral diffusion problem is the dipolar interaction induced nuclear spin flip-flops although for the GaAs quantum dot system, we have also included the indirect exchange interaction between the nuclear spins which turns out to be quantitatively comparable to the dipolar contribution to spectral diffusion. Our results are formally exact, and our numerical calculations provide an essentially exact (to better than 0.1% of the initial value) quantitative description of the Hahn spin echo decay. The significance of our quantum theory lies in the fact that, unlike all other theoretical descriptions of spectral diffusion spanning the last fifty years, we do not make any *ad hoc* phenomenological stochastic approximation in dealing with the non-Markovian spin dynamics in the spectral diffusion phenomena. We solve the problem essentially exactly using a quantum cluster decomposition technique, which is then theoretically justified by carrying out calculations to higher orders and by comparing with two independent perturbation techniques (i.e. the tau expansion and the dipolar perturbation theory). Very recently, a completely independent verification of our theory and results has appeared in the literature [13].

We note that spectral diffusion induced decoherence cannot be characterized by a simple  $T_2$  time since the

Hahn echo decay is not a simple exponential, and in fact, obeys different temporal power laws in the Si:P and the GaAs quantum dot systems. The spectral diffusion is a pure dephasing process arising from the temporal (non-Markovian) magnetic field fluctuations at the localized electron spin due to the nuclear spin dynamics, but it cannot be parameterized by a single  $T_2$  time except as a crude approximation. Within this crude approximation, we find the spectral diffusion induced  $T_2$  to be about  $100 \mu\text{s}$  for the Si:P system and about  $10 \mu\text{s}$  for the GaAs quantum dot system. But, this  $T_2$  can be enhanced indefinitely (up to tens of milliseconds) in the Si:P system through the isotopic purification of Si (i.e. by removing  $^{29}\text{Si}$  nuclei from the system) whereas in the GaAs quantum dots,  $T_2 \sim 10 \mu\text{s}$  is essentially an absolute upper limit (when using simple Hahn echo refocusing) since *all* Ga and As nuclei isotopes have free spins contributing to the spectral diffusion and isotopic purification is impossible. It is important to emphasize here that although spin polarizing the nuclei (e.g. through the dynamic nuclear polarization technique) would, in principle, suppress the nuclear induced spectral diffusion decoherence of electron spin, in practice, this would lead only to rather small enhancement of electron spin coherence since the presence of even a few nuclei with the “wrong” spin would cause nuclear pair flip-flop processes.<sup>34</sup>

Finally, we comment on the fact that the spectral diffusion process is quite a generic and general phenomenon in *any* spin decoherence problem with coupled spin dynamics (e.g. electron and nuclear spins, different types of nuclear spins, etc.) where the dynamics of one spin species has non-trivial (i.e. non-Markovian) temporal effects on the evolution of the spin dynamics of the other species. For example, a trivial (but not often emphasized in the literature) consequence of spectral diffusion consideration implies that in systems (e.g. Si:P; GaAs quantum dots) of interest to quantum computer architectures, the single flip of the localized electron spin will immediately decohere *all* the nuclear spins in its vicinity. Thus, the nuclear spin  $T_2$  time in these systems can at most be the  $T_1$  time for the electron spin! The typical low-temperature  $T_1$  time for electron spins in the GaAs quantum dots has been measured to be 1 ms or so, and therefore the nucleus spin  $T_2$  time would at most be 1 ms in the GaAs quantum dots, at least in the neighborhood of the localized electrons in the dot. The same consideration applies to the Si:P system. We believe that the general quantum theoretical techniques developed in this paper will be helpful in the studies of the temporal dynamics of other coupled spin systems wherever one spin species could act as a “decoherence bath” for the other system.

## APPENDIX A: HAHN ECHO ANALYSIS

Here we derive Eq. (15) from Eq. (10) and related equations. By noting that

$$S_x + iS_y = S_+ = |1_e\rangle\langle 0_e|, \quad (\text{A1})$$

we may rewrite Eq. (10),

$$v_E(\tau) = 2 |\text{Tr}_n(\langle 0_e | \rho(\tau) | 1_e \rangle)|, \quad (\text{A2})$$

where the  $n$  subscript in  $\text{Tr}_n$  denotes a trace over the nuclear subspace.

In addition to this equation, we will be referring to Eqs. (1)-(3), (5), (7), and (11)-(14). Repeated here, we have,

$$\rho(\tau) = U(\tau)\rho_0U^\dagger(\tau), \quad (\text{A3})$$

$$U(\tau) = e^{-i\mathcal{H}\tau}\sigma_{x,e}e^{-i\mathcal{H}\tau}, \quad (\text{A4})$$

$$\rho_0 = |\chi_e^0\rangle\langle\chi_e^0| \otimes \frac{e^{-\mathcal{H}_n/k_B T}}{M}, \quad (\text{A5})$$

$$|\chi_e^0\rangle = \frac{1}{\sqrt{2}}(|0_e\rangle + e^{i\phi}|1_e\rangle), \quad (\text{A6})$$

and

$$\mathcal{H} = \mathcal{H}_{Ze} + \mathcal{H}_{Zn} + \mathcal{H}_A + \mathcal{H}_B, \quad (\text{A7})$$

$$\mathcal{H}_{Ze} = \gamma_S B S_z, \quad (\text{A8})$$

$$\mathcal{H}_{Zn} = B \sum_n \gamma_n I_{nz}, \quad (\text{A9})$$

$$\mathcal{H}_A = \sum_n A_n I_{nz} S_z, \quad (\text{A10})$$

$$\mathcal{H}_B = \sum_{n \neq m} b_{nm} (\delta(\gamma_n - \gamma_m) I_{n+} I_{m-} - 2 I_{nz} I_{mz}). \quad (\text{A11})$$

First we note that  $\mathcal{H}_{Ze}$  commutes with the rest of the Hamiltonian and that  $\mathcal{H}_{Zn}$  commutes with  $\mathcal{H}_A$  (since an operator commutes with itself and any operator that acts on an orthogonal state space).  $\mathcal{H}_{Zn}$  also commutes with  $\mathcal{H}_B$  (and therefore commutes with the entire Hamiltonian). This is proven by noting that  $\mathcal{H}_B$  preserves the overall polarization of like nuclear spins. That is,

$$[\gamma_n I_{nz} + \gamma_m I_{mz}, \delta(\gamma_n - \gamma_m) I_{n+} I_{m-}] = 0. \quad (\text{A12})$$

Let us define

$$U_0(t) = e^{-i\mathcal{H}t}, \quad (\text{A13})$$

and exploit the above commutation relations to write,

$$U_0(t) = e^{-i\mathcal{H}_{Zn}t} e^{-i\mathcal{H}_{Ze}t} U'_0(t), \quad (\text{A14})$$

$$U'_0(t) = e^{-i(\mathcal{H}_A + \mathcal{H}_B)t}. \quad (\text{A15})$$

Using

$$\{\sigma_{x,e}, S_z\} = 0 \Rightarrow \sigma_{x,e} e^{-i\mathcal{H}_{Ze}\tau} = e^{i\mathcal{H}_{Ze}\tau} \sigma_{x,e}, \quad (\text{A16})$$

and the fact that  $\mathcal{H}_{Zn}$  commutes with  $\sigma_{x,e}$  (the former acting only on the nuclear spins and the latter acting on the electron spin), we can rewrite Eq. (A4)

$$U(\tau) = U_0(\tau)\sigma_{x,e}U_0(\tau) \quad (\text{A17})$$

$$= U'_0(\tau)\sigma_{x,e}U'_0(\tau)e^{-i\mathcal{H}_{Zn}(2\tau)} \quad (\text{A18})$$

$$= U'(\tau)e^{-i\mathcal{H}_{Zn}(2\tau)}, \quad (\text{A19})$$

$$U'(\tau) = U'_0(\tau)\sigma_{x,e}U'_0(\tau). \quad (\text{A20})$$

We can then rewrite Eq. (A3)

$$\rho(\tau) = U'(\tau)e^{-i\mathcal{H}_{Zn}(2\tau)}\rho_0e^{i\mathcal{H}_{Zn}(2\tau)}U'^\dagger(\tau), \quad (\text{A21})$$

$$= U'(\tau)\rho_0U'^\dagger(\tau), \quad (\text{A22})$$

using the fact that  $\mathcal{H}_{Zn}$  commutes with  $\rho_0$  (since it commutes with  $|\chi_e^0\rangle\langle\chi_e^0|$ , and  $\mathcal{H}_n = \mathcal{H}_{Zn} + \mathcal{H}_B$ ).

At this point it is convenient, for clarity, to write our operators as block matrices in the electron spin  $z$  basis. First we have, from Eq. (A15)

$$U'_0(\tau) = \begin{bmatrix} U_+ & 0 \\ 0 & U_- \end{bmatrix}, \quad (\text{A23})$$

where

$$U_\pm = e^{-i\mathcal{H}_\pm\tau}; \quad U_\pm^\dagger = e^{i\mathcal{H}_\pm\tau}, \quad (\text{A24})$$

with,

$$\mathcal{H}_\pm = \mathcal{H}_B \pm \mathcal{H}_{An}, \quad (\text{A25})$$

$$\mathcal{H}_{An} = \frac{1}{2} \sum_n A_n I_{nz}. \quad (\text{A26})$$

$U_\pm$  can be interpreted as the evolution operators of the nuclei with the electron spin constrained to be up or down respectively and ignoring the external magnetic field. Although  $U_+$  and  $U_-$  are function of  $\tau$ , we have dropped this as an explicit parameter for convenience.

In this same electron spin basis, we can write

$$|\chi_e^0\rangle\langle\chi_e^0| = \frac{1}{2} \begin{bmatrix} 1 & e^{i\phi} \\ e^{-i\phi} & 1 \end{bmatrix}, \quad \sigma_{x,e} = \begin{bmatrix} 0 & 1 \\ 1 & 0 \end{bmatrix}, \quad (\text{A27})$$

in order to obtain, from Eqs. (A5), (A22), (A20), and (A23),

$$\langle 0_e | \rho(\tau) | 1_e \rangle = \frac{e^{i\phi}}{2M} U_- U_+ e^{-\mathcal{H}_n/T} U_-^\dagger U_+^\dagger. \quad (\text{A28})$$

Plugging this into Eq. (A2) gives

$$v_E(\tau) = \frac{1}{M} \left| \text{Tr} \left\{ U_- U_+ e^{-\mathcal{H}_n/k_B T} U_-^\dagger U_+^\dagger \right\} \right|. \quad (\text{A29})$$

## APPENDIX B: FACTORING SUBSET CONTRIBUTIONS INTO CLUSTER CONTRIBUTIONS

A subset contribution is the product of its cluster contributions by the following proof. Let  $\mathcal{D}$  be the union of

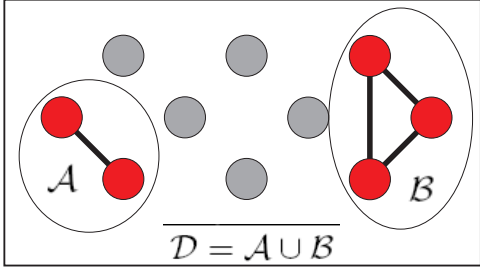


FIG. 15: This schematic represents a subset  $\mathcal{D}$  composed of clusters  $\mathcal{A}$  and  $\mathcal{B}$ . The circles represent nuclei. The red/dark circles denote nuclei contained in this subset.

clusters  $\mathcal{A}$  and  $\mathcal{B}$  that are disconnected from each other. This is shown in the schematic of Fig. 15. The states of the nuclei in  $\mathcal{A}$  and those of the nuclei in  $\mathcal{B}$  form separate vector spaces that are not coupled by  $\mathcal{H}_{\pm}$ . We can therefore, referring to Eq. (18) and defining  $U_{\mathcal{S}}$  for any  $\mathcal{S}$  such that  $v_{\mathcal{S}} = \text{Tr}(U_{\mathcal{S}})/M$ , note that  $U_{\mathcal{D}} = U_{\mathcal{A}} \otimes U_{\mathcal{B}}$ . Then,

$$v_{\mathcal{D}}(\tau) = \frac{\text{Tr}(U_{\mathcal{D}})}{M_{\mathcal{D}}} = \frac{\text{Tr}(U_{\mathcal{A}})}{M_{\mathcal{A}}} \frac{\text{Tr}(U_{\mathcal{B}})}{M_{\mathcal{B}}} \quad (\text{B1})$$

$$= v_{\mathcal{A}}(\tau)v_{\mathcal{B}}(\tau). \quad (\text{B2})$$

We will now use induction to prove that  $v'_{\mathcal{D}}(\tau) = v'_{\mathcal{A}}(\tau)v'_{\mathcal{B}}(\tau)$  as well. Invoking Eq. (20), we have

$$v_{\mathcal{D}}(\tau) = v_{\mathcal{A}}(\tau)v_{\mathcal{B}}(\tau) = \left( \sum_{\mathcal{S}_{\mathcal{A}} \subseteq \mathcal{A}} v'_{\mathcal{S}_{\mathcal{A}}}(\tau) \right) \left( \sum_{\mathcal{S}_{\mathcal{B}} \subseteq \mathcal{B}} v'_{\mathcal{S}_{\mathcal{B}}}(\tau) \right). \quad (\text{B3})$$

Assuming our hypothesis is true for smaller subsets than  $|\mathcal{D}|$ , we may write

$$\sum_{\mathcal{S} \subseteq \mathcal{D}} v'_{\mathcal{S}}(\tau) = \left( \sum_{\mathcal{S}_{\mathcal{A}} \subseteq \mathcal{A}} v'_{\mathcal{S}_{\mathcal{A}}}(\tau) \right) \left( \sum_{\mathcal{S}_{\mathcal{B}} \subseteq \mathcal{B}} v'_{\mathcal{S}_{\mathcal{B}}}(\tau) \right) \quad (\text{B4})$$

$$= v_{\mathcal{D}}(\tau) - v'_{\mathcal{A}}(\tau)v'_{\mathcal{B}}(\tau). \quad (\text{B5})$$

Thus from Eq. (21),

$$v'_{\mathcal{D}}(\tau) = v_{\mathcal{D}}(\tau) - \sum_{\mathcal{S} \subseteq \mathcal{D}} v'_{\mathcal{S}}(\tau) \quad (\text{B6})$$

$$= v'_{\mathcal{A}}(\tau)v'_{\mathcal{B}}(\tau). \quad (\text{B7})$$

The induction hypothesis was needed to obtain Eq. (B4). We can establish the base case by noting that a subset composed of two disconnected nuclei gives no contribution and neither does a cluster of size one. The induction is now complete.

### APPENDIX C: COMPUTATION OF TAU-EXPANSION COEFFICIENTS

Given an algebraic expression for a particular order, in  $\tau$ , of  $v_E(\tau)$ , as obtained according to section V A 1, we

need to compute numerical coefficients for specific applications (with explicit values of  $A_n$  and  $b_{nm}$ ). For a problem that has  $N$  non-trivial nuclei and an algebraic expression that has  $m$  terms and  $k$  summation labels, this will in general take  $O(mN^k)$  time to compute. This is a huge improvement over direct methods of evolving the state or diagonalizing the Hamiltonian since there are  $O(M = (2I + 1)^N)$  states of the system. So this expansion already saves us from calculations that grow exponentially with  $N$ . However, when  $N$  is on the order of 1000, which is actually a low estimate for considered applications, and we want the  $O(\tau^{10})$  term which has  $k = 5$ ,  $N^k$  is still quite large ( $10^{15}$ ). The situation can be drastically improved once more if we are willing to make another approximation which is very reasonable. We can set a threshold for values of  $|b_{nm}|$ , taking any  $|b_{nm}|$  below this threshold to be zero. Since  $|b_{nm}|$  generally decreases as nuclei are further separated, this amounts to a near neighbor approximation (also exploited by our cluster method). We can then adjust this threshold until convergence is achieved.

Let us say that our threshold is set such that, on average, each nuclei couples to  $L$  other nuclei. If we assume that all of the terms of the expression to be calculated are connected, not disjoint, graphs when representing labels as vertices and factors of  $b_{nm}$  as edges (as discussed in section V A 1 in the context of checking for like terms), then this approximation reduces the computation time to  $O(mNL^{k-1})$ . For the first label, there are  $N$  possible nuclei to which it can be assigned, but each additional label must be one of the  $O(L)$  vertices connected by an edge to a previous vertex/label.

Not all of the terms, in general, have these connected graph representations, however. Some of them are disjoint. This does not create a real problem though. These “disjoint” terms can be factored and dealt with separately. As a simple example,

$$\sum_{i,j,k,l}^{\text{distinct}} b_{ij}b_{kl} = \sum_{i \neq j} b_{ij} \sum_{k \neq l} b_{kl} - 2 \sum_{i \neq j} b_{ij}^2 - 4 \sum_{i,j,k}^{\text{distinct}} b_{ij}b_{jk}, \quad (\text{C1})$$

where the summation on the left (and one of them on the right) is over distinct indices as indicated above the summation symbol. The second term on the right has the factor of 2 because it includes  $b_{ij}b_{ji} = b_{ij}^2$  (since  $b_{nm} = b_{mn}$ ). The last term gets a factor of 2 from  $b_{jk} = b_{kj}$  and another factor of 2 from

$$\sum_{i,j,k}^{\text{distinct}} b_{ij}b_{ik} = \sum_{i,j,k}^{\text{distinct}} b_{ji}b_{jk} = \sum_{i,j,k}^{\text{distinct}} b_{ij}b_{jk}, \quad (\text{C2})$$

in which we relabelled indices.

Our computer program, described in section V A 1, automatically performs these conversions as a pre-process before being fed to the program that performs the numerical calculations. In addition to this conversion for

“disjoint” terms, the preprocessor performs a simple unidirectionally cascading factorization, for example of the form  $a(c+d(e+f))$  but not  $(a+b)(c+d)$ , which reduces the number of multiplications that must be performed in

the calculation. This factorization does not change the time complexity of the calculation, which is  $O(mNL^{k-1})$ , but it does provide a noticeable speedup.

---

<sup>1</sup> B. Herzog and E.L. Hahn, Phys. Rev. **103**, 148 (1956); A.M. Portis, Phys. Rev. **104**, 584 (1956).

<sup>2</sup> G. Feher and E.A. Gere, Phys. Rev. **114**, 1245 (1959).

<sup>3</sup> W.B. Mims and K. Nassau, Bull. Am. Phys. Soc. **5**, 419 (1960); W.B. Mims, K. Nassau, and J.D. McGee, Phys. Rev. **123**, 2059 (1961).

<sup>4</sup> J.R. Klauder and P.W. Anderson, Phys. Rev. **125**, 912 (1962).

<sup>5</sup> G.M. Zhidomirov and K.M. Salikhov, Sov. Phys. JETP **29** 1037 (1969).

<sup>6</sup> M. Chiba and A. Hirai, J. Phys. Soc. Japan **33**, 730 (1972).

<sup>7</sup> B.E. Kane, Nature **393**, 133 (1998).

<sup>8</sup> D. Loss and D.P. DiVincenzo, Phys. Rev. A **57**, 120 (1998).

<sup>9</sup> R. de Sousa and S. Das Sarma, Phys. Rev. B **68**, 115322 (2003).

<sup>10</sup> A.M. Tyryshkin and S.A. Lyon, Private communication; A.M. Tyryshkin *et al.*, Phys. Rev. B **68**, 193207 (2003).

<sup>11</sup> E. Abe, K.M. Itoh, J. Isoya and S. Yamasaki, Phys. Rev. B **70**, 033204 (2004).

<sup>12</sup> W.M. Witzel, R. de Sousa, and S. Das Sarma, Phys. Rev. B **72**, 161306(R) (2005).

<sup>13</sup> Wang Yao, Private communication; Wang Yao, Ren-Bao Liu, and L. J. Sham, cond-mat/0508441 (2005).

<sup>14</sup> R. de Sousa and S. Das Sarma, Phys. Rev. B **67**, 033301 (2003).

<sup>15</sup> R. F. Shulman, B. J. Wyluda, and H. J. Hrostowski, Phys. Rev. **109**, 808 (1958)

<sup>16</sup> N. Bloembergen and T. J. Rowland, Phys. Rev. **97**, 1679 (1955)

<sup>17</sup> R. K. Sundfors, Phys. Rev. **185**, 458 (1969)

<sup>18</sup> N. Shenvi, R. de Sousa, and K. B. Whaley, Phys. Rev. B **71**, 224411 (2005).

<sup>19</sup> E.L. Hahn, Phys. Rev. **80**, 580 (1950).

<sup>20</sup> J.M. Elzerman *et al.*, Nature **430**, 431 (2004); M. Xiao *et al.*, Nature **430**, 435 (2004); D. Rugar *et al.*, Nature **430**, 329 (2004).

<sup>21</sup> J.R. Petta *et al.*, Science, **309**, 2180 (2005).

<sup>22</sup> R. de Sousa, unpublished.

<sup>23</sup> X. Hu, R. de Sousa, and S. Das Sarma, cond-mat/0108339 (2001).

<sup>24</sup> H.Y. Carr and E. M. Purcell, Phys. Rev. **94**, 630 (1954); S. Meiboom and D. Gill, Rev. Sci. Instrum. **29**, 6881 (1958)

<sup>25</sup> A.V. Khaetskii, D. Loss, L. Glazman Phys. Rev. Lett. **88**, 186802 (2002).

<sup>26</sup> W.A. Coish and D. Loss, Phys. Rev. B **70**, 195340 (2004);

<sup>27</sup> C.P. Slichter, *Principles of Magnetic Resonance*, 3rd Ed. (Springer-Verlag, Berlin, 1990).

<sup>28</sup> C. Kittel, *Introduction to Solid State Physics*, 7th ed. (John Wiley & Sons, Inc., New York, 1996).

<sup>29</sup> A. Abragam, *The Principles of Nuclear Magnetism* (Oxford University Press, London, 1961), chapter IV, Eq. (63).

<sup>30</sup> S. Saikin, L. Fedichkin, Phys. Rev. B **67**, 161302(R) (2003).

<sup>31</sup> E. Yablonovitch *et al.*, Proc. of the IEEE, **91**, 761 (2003).

<sup>32</sup> CRC *Handbook of Chemistry and Physics*, 70th ed., E-82 (CRC Press, Boca Raton, Florida, 1989).

<sup>33</sup> D. Paget, G. Lampel, B. Sapoval, and V.I. Safarov, Phys. Rev. B, **15**, 5780 (1977).

<sup>34</sup> S. Das Sarma, Rogerio de Sousa, Xuedong Hu, Belita Koiller, Solid State Communications, **133**, 737 (2005).